Title

CSDE1 is a Post-Transcriptional Regulator of the LDL Receptor

Authors

Geoffrey A. Smith, MD PhD[†,1,2]; Arun Padmanabhan, MD PhD[†,3,4,5]; Bryan H. Lau, BS[6]; Akhil Pampana, MS[7,8]; Li Li, BS[9]; Y. Clara Lee, BA[5]; Angelo Pelonero, MS[5]; Tomohiro Nishino, MD PhD[5]; Nandhini Sadagopan, MS[3,4,5]; Rajan Jain, MD[9,10]; Pradeep Natarajan, MD[7,8,11]; Roland S. Wu, MD[3,4,6,12]; Brian L. Black, PhD[6]; Deepak Srivastava, MD[5,13,14]; Kevan M. Shokat, PhD[1,15]; John S. Chorba, MD*[,4,16]

[†]Drs. Smith and Padmanabhan contributed equally.
*Corresponding Author

Author Affiliations

[1]Department of Cellular and Molecular Pharmacology, University of California, San Francisco CA
[2]Present Affiliation: Boston Children's Hospital, Boston MA
[3]Division of Cardiology, UCSF Health, San Francisco CA
[4]Department of Medicine, University of California, San Francisco CA
[5]Gladstone Institute of Cardiovascular Disease, San Francisco CA
[6]Cardiovascular Research Institute, University of California San Francisco
[7]Cardiovascular Research Center, Massachusetts General Hospital, Boston MA
[8]Program in Medical and Population Genetics, Broad Institute of Harvard and MIT, Cambridge MA
[9]Department of Medicine and Penn Cardiovascular Institute, University of Pennsylvania, Philadelphia PA
[10]Department of Cell and Developmental Biology, Institute of Regenerative Medicine, and Penn Epigenetics Institute, University of Pennsylvania, Philadelphia PA
[11]Department of Medicine, Harvard Medical School, Boston MA
[12]Present Affiliation: Amgen, South San Francisco CA
[13]Departments of Pediatrics, and Biochemistry and Biophysics, University of California, San Francisco CA
[14]Roddenberry Center for Stem Cell Biology and Medicine at Gladstone, San Francisco CA
[15]Howard Hughes Medical Institute, University of California, San Francisco CA
[16]Division of Cardiology, Zuckerberg San Francisco General Hospital, San Francisco CA

Corresponding Author

John S. Chorba MD
600 16th St
Genentech Hall N514, MC2280
San Francisco CA 94143
phone: 415-601-7361
email: john.chorba@ucsf.edu

Abstract

The low-density lipoprotein receptor (LDLR) controls cellular delivery of cholesterol and clears LDL from the bloodstream, protecting against atherosclerotic heart disease, the leading cause of death in the United States. We therefore sought to identify regulators of the LDLR beyond the targets of current clinical therapies and known causes of familial hypercholesterolemia. We show that Cold Shock Domain-Containing Protein E1 (CSDE1) enhances hepatic *LDLR* mRNA decay via its 3' untranslated region to regulate atherogenic lipoproteins *in vivo*. Using parallel phenotypic genome-wide CRISPR interference screens, we found 40 specific regulators of the LDLR left unidentified by observational human genetics. Among these, we show that CSDE1 regulates the LDLR at least as strongly as the mechanistically distinct pathways exploited by the best available clinical therapies: statins and PCSK9 inhibitors. Additionally, we show that hepatic gene silencing of *Csde1* treats diet-induced dyslipidemia in mice better than that of *Pcsk9*. Our results reveal the therapeutic potential of manipulating a newly identified key factor in the post-transcriptional regulation of the *LDLR* mRNA for the prevention of cardiovascular disease. We anticipate that our approach of modelling a clinically relevant phenotype in a forward genetic screen, followed by mechanistic pharmacologic dissection and *in vivo* validation, will serve as a generalizable template for the identification of therapeutic targets in other human disease states.

Keywords

Atherosclerosis, cholesterol metabolism, CRISPR interference, CSDE1, genome-wide CRISPR screen, post-transcriptional regulation, LDL receptor, mRNA decay, pharmacogenetics, transferrin receptor

One Sentence Summary

A genome-wide CRISPR screen identifies CSDE1 as a key regulator of hepatic *LDLR* mRNA decay *in vivo*, making it a promising target for heart disease.

73 **Graphical Abstract**
74

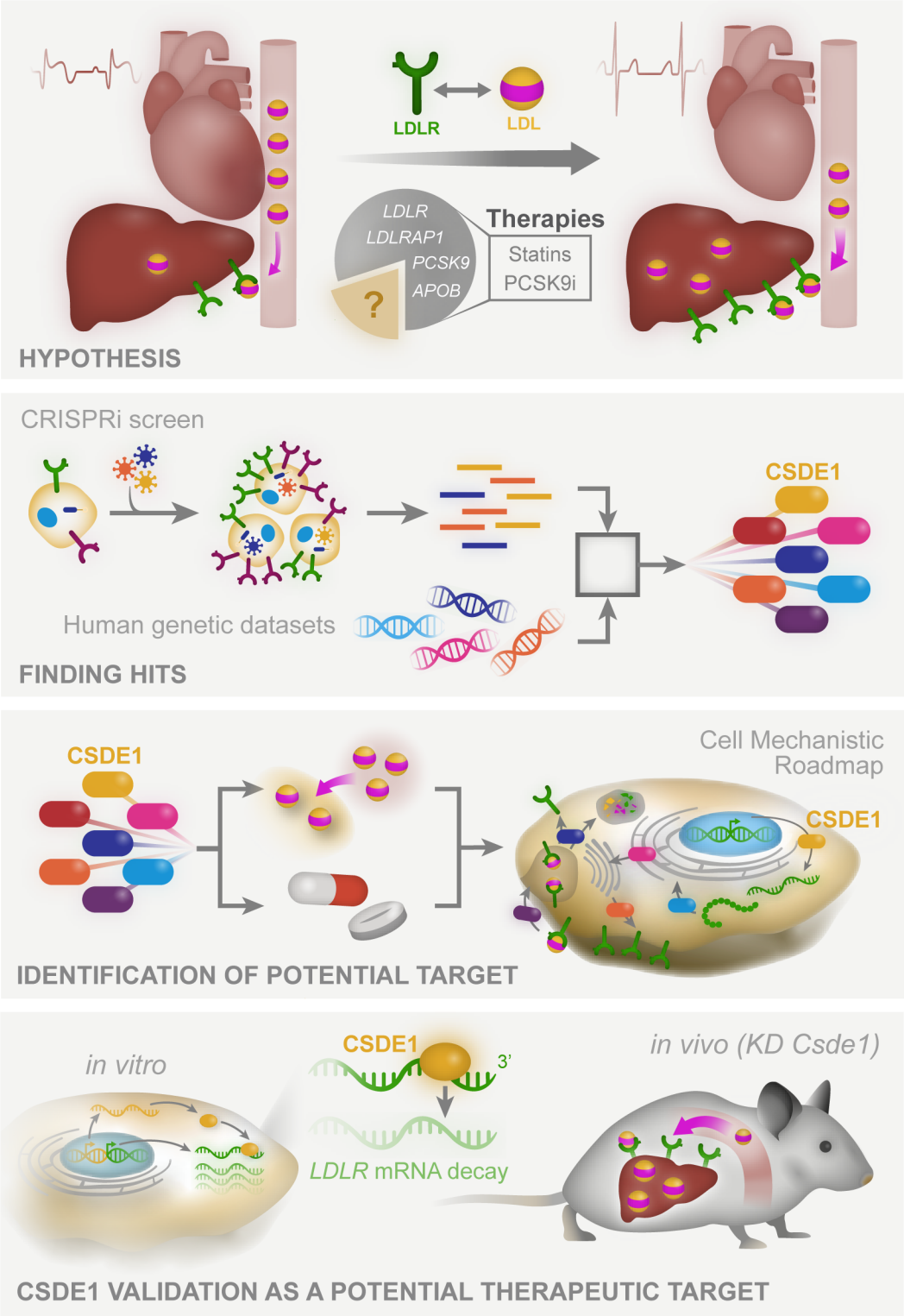

75
76
77

Introduction

The low-density lipoprotein receptor (LDLR) delivers cholesterol from low-density lipoprotein (LDL) to cells to maintain membrane homeostasis *(1)*. By clearing atherogenic LDL from the bloodstream, the hepatic LDLR protects against atherosclerotic heart disease *(2, 3)*. Despite successful therapies that upregulate the hepatic LDLR and reduce heart attacks *(4)*, cardiovascular disease remains the leading cause of death in Western countries *(5)*. Lowering LDL beyond the levels achieved by HMG-CoA reductase inhibitors (statins) improves clinical outcomes without adverse effects *(6, 7)*. Though there is a theoretical level at which LDL could get too low *(8)*, this has yet to be discovered in large randomized trials *(9, 10)*. Whether other LDLR regulatory mechanisms could be leveraged to further treat heart disease remains unknown.

The genetics of familial hypercholesterolemia (FH), which manifests as an isolated elevation in serum LDL, underlies the clinical success of LDLR upregulation by statins and PCSK9 inhibitors. Estimates suggest that 20-40% of FH phenotypes remain unexplained outside of the four major causes: *LDLR*, *APOB*, *PCSK9*, and *LDLRAP1 (11, 12)*. This implies that additional regulators of the LDLR exist. Advances in forward genetics *(13–15)* can now enable searches for tissue and disease-specific effects across the entire genome that may elude the sporadic natural variants found in observational studies, which themselves require compatibility throughout the entire lifespan and in all cell types. Moreover, hepatic delivery of gene silencing agents is effective in the clinic *(16)*, providing a therapeutic modality against hits whose phenotypes are driven by expression in the liver. We therefore employed a genome-wide CRISPR interference screen for factors involved in hepatic LDLR regulation, both to understand the biology of this important receptor and to uncover potential therapeutic targets in cardiovascular disease.

Results

A Genome-Wide CRISPR Interference Screen for LDL Receptor Regulation

We engineered the HepG2 cell line, which models the regulation of the LDLR *(17)*, to constitutively express a dCas9-KRAB fusion protein, enabling the knockdown of any given gene with an appropriate sgRNA (Fig. 1A) *(13, 14, 18)*. Because statins *(19, 20)* and PCSK9 inhibitors *(21–23)* increase cell surface LDLR, we scored surface LDLR levels. To focus on factors that preferentially affect the LDLR over other receptors, we performed a parallel screen for regulators of the transferrin receptor (TFR). This critical player in iron metabolism shares a clathrin-mediated intake mechanism, but is otherwise orthogonally regulated from the LDLR *(24, 25)*. Prior to our screen, we confirmed both dCas9-KRAB activity and an appropriate dynamic range for both LDLR and TFR regulation by transduction with sgRNAs expected to alter receptor levels in either direction (Fig. S1) *(26, 27)*.

We next performed our pooled screens in parallel by transducing a library encoding sgRNAs with 5-fold coverage of the entire protein-coding human genome *(14)*. We then selected the cells at the upper and lower third of receptor abundance by FACS and quantified the sgRNAs for each population via deep sequencing (Fig. S2, Tables S1-S4). We compared the degree of enrichment of LDLR or TFR surface levels in the high abundance to the low abundance cells (defined as ρ, Fig. 1B). We also compared the high and low receptor abundance cells to the unsorted population (defined as τ or γ, respectively) and included these results in our final hit count. This resulted in 130 total hits for the LDLR and 186 hits for the TFR (Tables S5-S6). We hypothesized that hits with shared phenotypes would likely have global effects on surface receptors, leaving us with 117 hits specific for LDLR regulation (Fig. 1C, Table 1). Gene ontology (GO) analysis *(28)* revealed a 15-fold enrichment for cholesterol metabolism as a biologic process (11 total hits, $p = 5.7\times10^{-10}$), providing confidence that we recapitulated our

target biology. The hits also included 48 members of potentially druggable protein classes, including 29 with proposed enzymatic activity, and 22 hits were unclassified in GO databases (Fig. S3A).

Cross-referencing Human Genetic Datasets Identifies LDLR Regulators in vivo

We next compared genes associated with serum LDL cholesterol (LDL-C) from published genome-wide association studies (GWAS) *(29–31)* to our list of hits. Intriguingly, only 13 of these genes overlapped with our results (Fig. 1D), even when we relaxed our threshold for hit selection. To improve power for multiple hypothesis testing across the entire genome, we turned to 390,375 UK Biobank participants with genome-wide genotypes and known plasma lipids (Table S7) to search for variants associated with LDL-C amongst only our hits *(32)*. We filtered to nonsynonymous protein coding variants in these hits by a threshold minor allele frequency (>0.001) and minimum statistical significance (Table 2). For *BCAM*, we found both an association between higher LDL-C and a nonsense variant, along with bidirectional associations between LDL-C and missense variants, suggesting that this pathway may be tunable. We also found associations between elevated LDL-C and variants in *MSMO1*, *C6orf132*, *HNF4A*, and *TIMELESS*, suggesting that these hits may be functional in the human and warrant further evaluation. The results also suggest that the accessible "genomic space" of the CRISPRi and GWAS strategies is only partially overlapping.

Regulators of Surface LDL Receptor Abundance Affect Functional Uptake of LDL

To validate our screen results, we generated CRISPRi HepG2 cells harboring either of the two top-scoring sgRNAs for 77 of our hits as well as established controls. We preferentially tested hits with an increase in surface LDLR upon inhibition, as well as those with potentially druggable functions or lacking associated GO terms. Since surface receptor levels might not necessarily correlate to increased function, we evaluated both LDLR and TFR surface phenotypes alongside a functional assay of LDL uptake *(33)*. Lastly, as knockdowns could also cause growth phenotypes, we assayed the number of cells surviving to FACS analysis as a proxy for viability.

We recapitulated the phenotypes for receptor abundance for at least one of the guides in the majority of the hits (55 genes, 71% of those tested, Table S8). Moreover, for 40 of these genes, both sgRNAs independently validated, suggesting against an off-target effect. We visualized these hits based on their effects, at single cell resolution, on LDLR and TFR levels, the LDLR/TFR ratio, functional LDL uptake and number of cells surviving to analysis (Figs. 2, S3B). Notably, most knockdowns had independently validated effects on LDLR abundance and LDL uptake of similar or greater magnitude than our *HMGCR* or *PCSK9* controls.

Knockdown of hits expected to alter cellular cholesterol balance or transcriptionally regulate the LDLR showed directionally consistent effects between LDLR abundance and function (Fig. 2). For genes in the enzymatic pathway of cholesterol metabolism *(34)* (*HMGCS1* and *MSMO1*), this is consistent with activation of SREBP2-mediated *LDLR* transcription. For genes encoding certain transcription factors (*HNF1A (35)*, *HNF4A (36)*, *ONECUT1 (37)*, and *ZEB1 (38)*), this is consistent with an effect on *LDLR* transcription itself. Knockdowns of *SLC25A27*, which encodes a mitochondrial uncoupling protein *(39)*, and *ABCA4*, encoding a known lipid transporter *(40)*, both exhibited reductions in LDLR abundance and function (Fig. 2). These genes could plausibly induce a negative lipid balance, increasing LDL uptake via both LDLR dependent and independent mechanisms.

Targeting of hits that either affect multiple transcriptional pathways or regulate endocytosis showed opposite effects on LDLR abundance and function. Knockdown of *TRIB1*, a GWAS hit

(29) encoding a pseudokinase that regulates the COP1 E3 ligase *(41, 42)* and affects multiple transcription factors *(43)*, showed this phenotype. In the mouse, *TRIB1* overexpression lowers serum cholesterol, while the knockout has the opposite effect *(44, 45)*, consistent with our results. Knockdown of *AP2M1*, a TFR screen hit that encodes an adaptor protein required for endocytosis *(46)*, was similar, consistent with an accumulation of non-functional receptors at the cell surface. This phenotype, though specific to the LDLR, was also seen with knockdown of *BCAM*, which encodes a membrane cell adhesion molecule *(47)* identified by GWAS *(31)*, and *TMEM217*, which encodes an uncharacterized transmembrane protein (Figs. 2, S4). This suggests that these proteins could have a similar endocytosis adaptor function specific for the LDLR, akin to *LDLRAP1 (48)*, in which mutations cause a recessive form of FH.

Pharmacologic Inhibition of Clinically Relevant Pathways Provides Mechanistic Insight into Putative LDLR Regulators

We next turned to pharmacologic approaches to perturb specific pathways of LDLR regulation. We hypothesized that hits might alter cholesterol metabolism, LDLR recycling, or a yet unspecified pathway. By combining CRISPRi knockdown with either a statin, to inhibit endogenous cholesterol biosynthesis *(49, 50)*, or a PCSK9 inhibitor, to arrest LDLR lysosomal degradation *(23)*, and assessing the combined effect, we inferred mechanistic information about the target gene. Furthermore, we hypothesized that either additive or potentiating effects between a clinically validated therapy and a hit gene might suggest promising therapeutic targets.

We evaluated the receptor abundance and function phenotypes for 29 of our validated hits in the presence or absence of a statin *(51)* or PF-846, a selective inhibitor of PCSK9 translation *(52, 53)* (Fig. 3, Table S9). We calculated a synergy score by subtracting the differential effects of CRISPRi knockdown, compared to the control, in the presence of compound from that with the DMSO vehicle. A more positive value indicated synergy, and a more negative value indicated antagonism.

Upon knockdown, regulators of cholesterol biosynthesis (*SREBF2*, *HMGCR*, *HMGCS1*, *MSMO1*, and *PMVK*) showed antagonism with the statin, but mild synergy with PCSK9 inhibition (Fig. 3). This is consistent with the SREBP2-mediated *PCSK9* transcription that underlies the clinical synergy between statins and PCSK9 inhibitors. The synergy phenotypes for knockdown of *MRPL16*, which encodes a structural component of the mitochondrial ribosome *(54)*, mirrored these cholesterol biosynthetic genes (Fig. 3), suggesting that MRP-L16 may play a role in the mitochondrial generation of metabolic precursors to sterol biogenesis. In contrast, *C6orf132* knockdown showed the opposite phenotype: mild synergy with a statin, and mild antagonism with PF-846 (Fig. 3). Given that C6orf132 localizes to the Golgi *(55)*, this suggests it may function by facilitating LDLR delivery to the cell surface, prior to any interaction with extracellular PCSK9. For some transcription factors, the synergy phenotypes can point to their downstream targets. For example, synergy of *HNF1A* knockdown with a statin (Fig. 3) is consistent with disruption of HNF1-α-mediated *PCSK9* transcription *(56)*.

CSDE1 Regulates the Stability of LDLR mRNA

One of our strongest hits, *CSDE1*, also known as upstream of N-ras (UNR), encodes an RNA binding protein with varied regulatory functions *(57–59)*, including mRNA decay *(60)*. As the *LDLR* 3' UTR consists of adenylate-uridylate (AU)-rich elements (AREs) implicated in mRNA stability *(61)*, we hypothesized that CSDE1 could mediate the degradation of the *LDLR* transcript, thereby explaining its observed receptor abundance, function, and synergy phenotypes.

In the setting of *CSDE1* knockdown, we observed progressively higher LDLR abundance with sterol depletion and a concomitant statin (Figs. 4A, S5A-C). This suggests the mechanism of *CSDE1* disruption is at least additive with SREBP2-mediated *LDLR* transcription and statin therapy. We also observed that overexpression of isoform 1 of CSDE1, but not isoforms 2 through 4, reduced surface LDLR in HepG2 cells (Figs. 4B, S6A-D). Overexpression of all four isoforms of CSDE1 downregulated LDLR levels in the *CSDE1* knockdown cells, though isoform 1 showed the strongest effect (Fig. S6E-I). The opposing directional effects of *CSDE1* knockdown and overexpression suggest that, under physiologic expression conditions, isoform 1 of CSDE1 is a rate-limiting regulator of the LDLR.

Consistent with our mechanistic hypothesis, we noted over a 2-fold increase in steady-state mRNA levels of *LDLR* (Fig. 4C), as well as depleted CSDE1 (Figs. 4C, S7), in the *CSDE1* knockdown cells. Among control mRNA targets, we also observed significant increases in *MYLIP* and *KHSRP* mRNA. These gene products downregulate the LDLR *(26, 62)*, which is the opposite of our observed phenotype, suggesting that the direct effect of *CSDE1* knockdown on the *LDLR* mRNA predominates. To specifically evaluate transcriptional decay, we treated cells with actinomycin D and measured *LDLR* transcript levels over time. We observed significantly higher *LDLR* mRNA in the *CSDE1* knockdown cells at all subsequent timepoints (Fig. 4D). The mRNA half-life, modeled by a single-phase decay equation, was nearly 1.5-fold longer for the *CSDE1* knockdowns compared to controls ($p = 0.0021$, Fig. 4D). Notably, *CSDE1* knockdown had no significant effect on *HMGCR*, *SREBF2*, *PCSK9*, or *TFRC* mRNA levels over time (Fig. S8), suggesting that the effect on mRNA stability was isolated to *LDLR* among our tested transcripts.

To probe the relationship of CSDE1 to the *LDLR* 3' UTR, we transiently expressed luciferase constructs (Fig. 4E) under control of the native *LDLR* promoter in the *CSDE1* knockdown cells. The luciferase-only constructs showed appropriate physiologic upregulation by sterols, regardless of *CSDE1* knockdown (Fig. S9). Constructs fused to the *LDLR* 3' UTR, but not those fused to the *LDLR* coding sequence alone, exhibited increased reporter activity with *CSDE1* knockdown (Fig. 4F). Notably, this increase in activity was attenuated by removing the first of four AREs *(61, 63)* from the 3' UTR (Fig. 4F). Activity of the 3' UTR-fused construct increased further with statin coadministration (Fig. 4G), suggesting that *CSDE1* knockdown may be synergistic with statins, consistent with our prior results (Fig. 3). Taken together, we conclude that under physiologic conditions, CSDE1 mediates decay of the *LDLR* mRNA through its 3' UTR, with the first ARE of the UTR required for its full effect.

Disruption of CSDE1 Upregulates the LDLR in vivo

We then turned to an *in vivo* model in zebrafish, as the 3' UTR of its ortholog *ldlra* (XM_005163870.4) is highly AU-rich and contains at least two canonical ARE sequences for mRNA regulation *(64)*. We employed yolk microinjection of a Cas9-ribonucleoprotein (RNP) complex containing redundant guides to achieve near-saturation gene disruption *(65)*, followed with dietary cholesterol supplementation, and evaluated total cholesterol in the larvae *(66)*. Targeting of *csde1* protected against cholesterol accumulation, with a modest (12%) but significant reduction in total cholesterol in 8-day post fertilization (dpf) zebrafish, without any obvious phenotypic abnormalities (Figs. 5A, S10). By contrast, targeting of *ldlra* showed the expected 1.4-fold increase in total cholesterol (Fig. 5A) *(66)*.

We next probed the effect of *Csde1* gene silencing in the mouse as a therapeutic proof-of-principle, given even greater homology between the 3' UTRs of the murine and human *LDLR* orthologs *(67)*. Using C57BL/6 mice on an atherogenic diet *(68)*, we delivered shRNA against *Csde1 (59)*, *Pcsk9*, or scramble control via low-dose adeno-associated virus 8 (AAV8). Two

weeks later, we observed a 25% reduction in fasting plasma cholesterol in the *Csde1* knockdown mice, which exceeded the effect of *Pcsk9* knockdown (Fig. 5B). We then re-dosed the *Csde1* and scramble AAV8-shRNA and, 2 weeks later, observed an even stronger phenotype (Fig. S11A). Lipoprotein fractionation of the mouse plasma showed that *Csde1* knockdown mostly affected the VLDL-containing fractions (Fig. 5C), consistent with upregulation of the murine LDLR on our dietary background *(69, 70)*. Accordingly, we observed an increase in *Ldlr* expression in the liver tissue of the *Csde1* knockdown mice (Fig. S11B). Notably, we observed no differences in appearance or behavior of the mice, nor in plasma levels of alanine aminotransferase activity (Fig. S11C), arguing against hepatic or systemic toxicity of either the *Csde1* shRNA or the gene knockdown.

To gain further insight, we performed bulk RNA sequencing on the liver tissue (Figs. 5D, S11D-F, Table S10). We compared the *Csde1* knockdown to control (scramble) mice, using the mice with the highest transcript counts of a vector-delivered eGFP reporter to control for variations in transduction efficiency. We then filtered our results for the differentially expressed transcripts in the control mice at the extremes of eGFP expression, to control for the effects of viral transduction alone. As expected, we found higher *Ldlr* expression in the *Csde1* knockdown mice ($\log_2$FC = 0.43, p = 0.0029, Table S10). Consistent with our mechanistic hypothesis, GO enrichment analysis of the differentially expressed genes revealed that mRNA processing was the most significantly downregulated biological process in the *Csde1* knockdown mice (OR = 2.7, adj. p = 0.0085, Figs. 5D, S11F, Table S11). Spliceosome complex assembly was also significantly downregulated (OR = 7.4, adj. p = 0.0085, Figs. 5D, S11F, Table S11).

Discussion

The powerful biology of the LDLR is unquestioned in cardiovascular medicine *(71)*. Since their introduction, statins, which upregulate the LDLR, have become a major public health success, and with the discovery of PCSK9 and the therapeutic antibodies targeting it, patients can safely reach much lower LDL levels than is achievable by statins alone *(10)*. Together, this suggests that we can push further on this LDL-LDLR axis and still achieve a clinical benefit.

In this study, we modeled a clinically relevant phenotype of LDLR abundance and function, complementing the independent investigations of other groups *(72, 73)*. When synthesizing our screening and validation data together with large-scale genomics and additional pharmacologic perturbations, we produce an exploratory map of potential regulatory mechanisms for the LDLR (Fig. 6). These data represent not just promising targets but also pathways likely to be impacted by therapies already in use in the clinic.

We have shown that *CSDE1*, one of our strongest hits, regulates LDLR levels in HepG2 cells by promoting *LDLR* mRNA decay via its 3' UTR. These data lay in concert with CSDE1's destabilizing effects on other transcripts, such as c-Fos *(60)*. We have also shown that *in vivo* knockdown of *Csde1* upregulates the hepatic LDLR and improves atherogenic lipid profiles in mice. This mimics the effect of deleting the 3' UTR *in vivo (74)* and illustrates the promise of targeting CSDE1 to lower LDL and protect against atherosclerosis. It is notable that several small molecules, including triciribine *(63)* and berberine *(67, 75)*, have stabilizing effects on *LDLR* mRNA, though whether their mechanisms directly involve CSDE1 remain to be elucidated. The magnitude of LDLR upregulation imparted by *CSDE1* knockdown mirrors or exceeds that of *HMGCR* and *PCSK9* in both tissue culture and mouse models, suggesting that a high-fidelity approach targeting CSDE1-mediated *LDLR* mRNA decay in the clinic could have similarly impressive effects. Additionally, our mechanistic data suggest that targeting CSDE1 would be at least additive with the use of statins.

The degree to which CSDE1 inhibition affects other transcripts, or other tissues *(59, 76)*, remains an important question. As an RNA chaperone, CSDE1 can have a variety of effects, from mRNA stabilization *(58)* to promotion or inhibition of translation *(77–80)*, dependent on the identity of the RNA it binds and the cofactors with which it interacts. Intriguingly, though CSDE1 was found to bind biotinylated *LDLR* 3' UTR transcripts in HepG2 cell lysates *(62)*, cross-linking immunoprecipitation approaches in both mouse brain and melanoma cells failed to identify *LDLR* mRNA as a CSDE1 binding partner *(81, 82)*. This suggests that the CSDE1-*LDLR* interaction is context dependent. Advances in liver-specific delivery of gene-silencing agents *(16, 83)*, novel gene editing technologies *(84)*, and small molecules *(85)* offer the possibility that selectively targeting hepatic CSDE1 for cholesterol lowering could avoid systemic toxicities.

Though we observed no toxicity, transcriptional profiling suggests that disrupting hepatic CSDE1 upregulates both apoptosis-related and GTPase-mediated signaling pathways (Figs. 5D, S11F, Table S11). Notably, CSDE1 appears to protect from apoptosis in both colorectal cancer *(86)* and Huh7 cells *(87)*. Though biologically plausible, we hesitate to make definitive conclusions from these data since the cholate-rich diet we used to obtain hyperlipidemia also causes liver inflammation and hepatic steatosis *(88)*. Despite this confounder, we expect that our transcriptomic analysis will guide further investigations of potential toxicities from hepatic CSDE1 disruption. Given that CSDE1 has such varied effects on other transcripts, future mechanistic dissection of the hepatic CSDE1-*LDLR* interaction could identify what makes this relationship unique and guide a potential therapeutic strategy. Combination therapies targeting interconnected pathways to disease can provide increased benefits without inducing extreme side effects, with angiotensin receptor blockade and neprilysin inhibition in heart failure a prominent clinical example *(89)*. Though speculative, we are intrigued by the effects of CSDE1 on mRNA splicing (Figs. 5D, S11F, Table S11), and we note in particular that the spliceosome helicase DDX39B was both validated as a regulator of the LDLR from our CRISPRi screen (Fig. 2, Table S8) and downregulated by *Csde1* knockdown *in vivo* ($\log_2$FC = -0.32, p = 0.011, Table S10). To the extent hepatic CSDE1 utilizes specific factors to downregulate *LDLR* mRNA, simultaneous tissue-specific drugging of both CSDE1 and these factors could widen the overall therapeutic window. We anticipate that our study will serve as the seed for these and other further investigations.

Methods

Study Design

We designed the study as a discovery biology experiment to identify new regulators of the LDL receptor. We used an established tissue culture model, HepG2 cells, to evaluate for LDL receptor regulation. We used wild-type zebrafish (Ekwill) and wild-type mice (C57BL/6) to validate the contribution of our top hit, CSDE1, to LDL receptor regulation *in vivo*. We evaluated sufficient cells for the LDLR and TFR screens to provide adequate coverage for transduction and downstream sequencing of each sgRNA in the genome-wide library. Sample sizes for animal experiments were estimated to provide 80% power (two-tailed α = 0.05) for a 25% effect in cholesterol levels compared to controls, based on effects in these models in the existing literature. The numbers of animals used in each experiment are noted in the figures and manuscript. Unless otherwise noted, all *in vitro* data are representative of multiple (≥ 3) experimental outcomes to ensure robust outcomes. Experiments were not performed in a blinded fashion. All animal studies were performed in accordance with IACUC approved protocols at the University of California, San Francisco.

Plasmids and Cloning

SFFV-dCas9-BFP-KRAB (Addgene 46911), CRISPRi/a v2 (Addgene 84832), pMD2.G, dR8.91, and the hCRISPRi v2 top5 sgRNA library (Addgene 83969) were gifts from L. Gilbert and J.

384 Weissman. Oligonucleotides of the protospacers of validated sgRNA sequences *(14)*, as well as
385 those for PCR amplification and isothermal assembly, were obtained from Elim
386 Biopharmaceuticals (Hayward CA). Protospacers were cloned into the CRISPRi/a v2 vector
387 using restriction enzyme digest (BlpI and BstXI, ThermoFisher, Waltham MA) and ligation with
388 10× T4 ligase (NEB, Ipswich MA). CSDE1 overexpression constructs were created by PCR
389 expansion of *CSDE1* (HsCD00949797, DNASU, Tempe AZ) or AcGFP1 (vector control,
390 pIRES2-AcGFP1, Clontech, Mountain View CA) and isothermal assembly *(90)* into the
391 pcDNA5/FRT/TO backbone (ThermoFisher), followed by site-directed mutagenesis to generate
392 the four CSDE1 isoforms (UniprotKB O75534 1 through 4). pLuc2-$Prom_{LDLR}$ was created by
393 PCR expansion of the target luciferase from pGL4Luc-RLuc (Addgene 64034), custom gene
394 synthesis of the LDLR promoter (NCBI Reference Sequence NG_009060.1, from -687 bp to the
395 *LDLR* start codon, Twist Biosciences, South San Francisco CA) and isothermal assembly into
396 the pcDNA5/FRT/TO backbone. pSS-NLuc was created by PCR expansion of the target
397 luciferase from pNL1.1 (Promega, Madison WI) into a vector containing the PCSK9 signal
398 sequence from the same backbone *(91)*. The remaining pLuc2-$Prom_{LDLR}$ constructs were
399 created by PCR expansion of the coding region of *LDLR* (HsCD00004643, DNASU), custom
400 gene synthesis of the 3' UTR of the *LDLR* mRNA (NCBI Reference Sequence
401 NM_001252658.1, Twist Biosciences), or custom oligonucleotides to add the P2A ribosomal
402 skipping linker *(92, 93)* and isothermal assembly into pLuc2-$Prom_{LDLR}$, as appropriate for each
403 construct. All plasmids were confirmed by Sanger sequencing. Expansion of the top5 sgRNA
404 library was as previously described *(13)*.
405
406 *Cell Culture and Lentiviral Production*
407 HepG2 (ATCC HB-8065) and derivatives were cultured in low-glucose DMEM (1 g/L,
408 ThermoFisher) with 10% FBS (Axenia BioLogix, Dixon CA), GlutaMax (ThermoFisher) and 1×
409 penicillin-streptomycin (ThermoFisher), and sent thrice through a 21g needle during passaging
410 to minimize cell clumping. HEK-293T (ATCC CRL-3216) were cultured in standard DMEM
411 (ThermoFisher) with 10% FBS. All cell lines were cultured at 37 °C at 5% CO_2, seeded for
412 approximately 50% confluency at the time of experiment, and were confirmed free of
413 *Mycoplasma* contamination by the MycoAlert PLUS Mycoplasma Detection Kit (Lonza,
414 Switzerland). Lentivirus was produced in 293T cells by transfection of dR8.91, pMD2.G, and the
415 appropriate pLKO-derived vector (at ratios of 8 µg, 1 µg, and 8 µg, respectively, per 15 cm dish)
416 with Trans-LT1 (Mirus Bio, Madison WI), according to the manufacturer's instructions. Viral
417 harvest media was supplemented with Viralboost (Alstem, Richmond CA), collected 2-3 days
418 after transfection, and filtered through 0.44 µm polyvinylidene difluoride filters and either frozen
419 for storage at -80 °C or used immediately for transduction.
420
421 *Generation of CRISPRi Cell Lines*
422 All cell lines were transduced using virus-containing supernatant in the presence of 8 µg/ml
423 polybrene (Millipore-Sigma, St. Louis MO). HepG2 expressing dCas9-KRAB were derived by
424 transduction with lentivirus harboring SFFV-dCas9-BFP-KRAB, followed by two rounds of FACS
425 for BFP-positive cells on a BD FACSAria II. dCas9-KRAB HepG2 with individual targeting
426 sgRNAs were derived by transduction with lentivirus harboring the desired sgRNA, followed by
427 48 hrs of puromycin selection (2 µg/ml, InvivoGen, San Diego CA), prior to experiments.
428
429 *Quantitative Real-Time PCR*
430 dCas9-KRAB HepG2 stably expressing an appropriate sgRNA were harvested, lysed, and total
431 RNA was extracted via the RNeasy Mini Kit (Qiagen, Germantown MD). RNA was converted
432 into cDNA using qScript cDNA SuperMix (QuantaBio, Beverly MA) following the manufacturer's
433 instructions. RT-qPCR was performed against indicated targets with PrimeTime qPCR primers
434 (IDT, Coralville IA) using the SYBR Select Master Mix (ThermoFisher) according to the

435 manufacturer's instructions on a CFX96 Touch Real-Time PCR Detection System (BioRad,
436 Hercules CA). Fold changes were calculated using ΔΔCt analysis, normalizing each sample to
437 *B2M* controls, using CFX Maestro software (BioRad).
438
439 *Receptor Abundance Analysis*
440 1-2 days prior to analysis, dCas9-HepG2 cells and derivatives were cultured in low-glucose
441 DMEM with 5% lipoprotein deficient serum (Kalen Biomedical, Germantown MD). Prior to
442 analysis, cells were dissociated with Accutase (Innovative Cell Technologies, San Diego CA),
443 collected, washed in PBS (ThermoFisher), live-dead stained with Ghost Dye Red 780 (1:1000
444 dilution, Tonbo Biosciences, San Diego CA), washed, and then stained with the indicated
445 antibody in FACS buffer (PBS with 1% FBS, 10 U/ml DNAse I, GoldBio, St. Louis MO) for 30
446 minutes on ice with gentle agitation. Cells were washed, resuspended in FACS buffer, filtered
447 through 90 µm mesh (Elko Filtering, Miami FL) to give a single cell suspension, and placed on
448 ice. Cells were then analyzed on either a BD Fortessa, BD LSRII, BD FACSAria II, or Beckman
449 Coulter CytoFLEX, or sorted on a BD FACSAria II, depending on the experiment. In general,
450 gating excluded cells positive for live-dead staining and included only the cells positive for the
451 level of BFP expression induced by the CRISPRi/a v2 vector. FACS analysis and figure
452 preparation was performed with FlowJo v10 (BD, Ashland OR).
453
454 *Genome-Wide CRISPRi Screen*
455 The screen was conducted similarly to prior descriptions *(13–15)*. Approximately 200×10^6
456 dCas9-KRAB HepG2 were transduced with hCRISPRi-v2 top 5 sgRNAs/gene lentivirus at an
457 MOI of ~0.5, and with polybrene at 8 µg/ml, on day 1. Cells were grown on 15-cm dishes,
458 subdivided into four replicates immediately upon transduction (biological duplicate for each
459 screen), and reseeded every 3-4 days as necessary to avoid overconfluence. Cells were
460 selected with puromycin (2 mg/ml) from day 2 through day 6. On day 5, cells for the LDLR sort
461 were placed in DMEM with lipoprotein depleted serum (5%). On day 7, approximately 50×10^6
462 cells from 2 replicates were live-dead stained and stained for LDLR as described above, and
463 then two-way sorted on a BD FACSAria II for the top and bottom 33% by LDLR abundance.
464 Cells were spun down, washed in PBS and frozen at -80 °C. On day 8, the sort was repeated
465 except in one replicate, cells were stained for TFR instead of LDLR and then sorted as per
466 above. Genomic DNA was isolated using a NucleoSpin Blood DNA extraction kit (Macherey-
467 Nagel, Bethlehem PA). The sgRNA-containing region was PCR-amplified with NEBNext Ultra II
468 Q5 MasterMix (NEB), acrylamide gel-purified, and size-selected by SPRI beads (Beckman
469 Coulter, Indianapolis IN), all as previously described, prior to sequencing on an Illumina HiSeq
470 4000.
471
472 *Screen Processing*
473 Sequencing data were aligned to the top5 library, counted, and quantified using the
474 ScreenProcessing pipeline (accessed from https://github.com/mhorlbeck/ScreenProcessing*(14)*
475 4/25/2019). Phenotypes and Mann-Whitney *P* values were determined as previously described
476 *(14)*, with the phenotypes defined as follows: ρ indicated the comparison in high-abundance vs.
477 low abundance cells, τ indicated the comparison in high-abundance vs. unsorted cells, and γ
478 indicated the comparison in low-abundance vs. unsorted cells. Counts from 4 guides were
479 removed from the final analysis as there was evidence of contamination from individually cloned
480 plasmids (PCSK9_+_55505255.23-P1P2, HMGCR_+_74633053.23-P1P2, TFRC_-
481 _195808987.23-P1P2, ACO1_-_32384733.23-P1P2). A hit threshold of 7 (normalized
482 phenotype z score $\times$ -log10(p-value) $\geq$ 7) *(13)* was used to identify hits from ρ, τ, and γ
483 phenotypes, which were then compiled. Identical analysis of the TFR screen was used to
484 prioritize hits unique to LDLR regulation. Gene ontology analysis was performed using the

PANTHER Classification System database (v15) *(28, 94)*. For relaxation of the hit threshold for comparison to GWAS studies, a score of 6 was used. Cellular localization of hits was imputed by manual curation from UniProt *(95)* and the Human Protein Atlas *(55)*.

Human Genomic Analysis

Protein coding variants for hits validated at the individual sgRNA level were assayed in the UK Biobank *(96)* for associations with LDL-C. In the setting of a statin medication, LDL-C was divided by 0.7 as before *(30)*. Genotyping and imputation was performed in the UK Biobank as previously described *(32)*, and nonsynonymous protein coding variants with minor allele frequencies greater than 0.001 were considered. Efficient linear mixed models adjusting for age, sex, genotyping array, and principal components of ancestry were employed, using BOLT-LMM *(97)*. Statistical significance was assigned at $\alpha = 0.05/117 = 0.000427$ to account for multiple hypothesis testing.

Validation Experiments of Individual sgRNAs

Cloning of protospacers, as described above, was performed in 96-well plate format until selecting individual colonies. Lentiviral production in 293T, transduction of dCas9-KRAB HepG2 with lentiviral sgRNA vectors, and receptor abundance and LDL uptake assays were similarly performed in 96-well plate format to maximize throughput.

LDL Uptake Assays

Assays were performed as previously described*(33)* with the following modifications. dCas9-HepG2 cells harboring individual sgRNAs were treated similarly to receptor abundance analysis, except that prior to harvest, cells were washed and then treated with 5 µg/ml 1,1'-dioctadecyl-3,3,3',3'-tetramethylindocarbocyanine perchlorate (DiI) labeled LDL (Kalen Biomedical) in low-glucose DMEM with 0.5% BSA (MilliporeSigma) for 1 hr at 37 °C. Cells were then washed, collected, and prepared for FACS analysis, as described above, but without antibody labelling.

Pharmacologic Synergy Experiments

Receptor and LDL uptake assays were performed as described, with cells treated overnight with either simvastatin (6 µM, MilliporeSigma), PF-6846 (10 µM, MilliporeSigma), or DMSO vehicle (final concentration of 0.5%) overnight prior to analysis. Synergy scores were calculated by the following equation:

$$\left(LDLR_{sgRNA+compound} - LDLR_{NegCtrl+compound}\right) - \left(LDLR_{sgRNA+vehicle} - LDLR_{NegCtrl+vehicle}\right)$$

with $LDLR$ obtained as the mean fluorescence, background subtracted from an unstained control and subsequently normalized to $LDLR_{NegCtrl+vehicle}$ within a given experiment.

Overexpression Experiments

HepG2 or engineered dCas9-HepG2 cell lines were seeded into 96 well plates at 5×10^4 cells per well in HepG2 growth medium. After 24 hrs, cells were washed and changed into low-glucose DMEM with 5% lipoprotein-deficient serum. Each well was transfected with 100 ng of the appropriate CSDE1 overexpression construct, or vector control, in a total of 10 µL OptiMEM (ThermoFisher) using Lipofectamine 3000 (ThermoFisher) according to the manufacturer's instructions. Cells were incubated at 37 °C with 5% CO_2 for 72 hrs, and then harvested for LDL receptor expression analysis as above.

mRNA Decay Experiments

534 Engineered dCas9-HepG2 cell lines harboring sgRNAs against CSDE1
535 (CSDE1_+_115300577.23-P1P2) or a negative control (Unassigned=negZNF335_-
536 _44601297.24-all) were seeded into 12 well plates at 5×10^5 cells per well in HepG2 growth
537 medium. After 24 hrs, cells were washed and changed into sterol-depleting media (low-glucose
538 DMEM with 5% lipoprotein-deficient serum) supplemented with 6 μM simvastatin. After an
539 additional 24 hrs, actinomycin D (MilliporeSigma) was added at 5 μg/ml, and cells were
540 harvested as described at the indicated timepoints.
541
542 *Immunoblots*
543 Engineered dCas9-HepG2 cell lines harboring appropriate sgRNAs were grown in growth
544 medium and harvested with 0.25% trypsin digestion. Cells were washed and lysed in lysis buffer
545 on ice (50 mM Tris-HCl pH 7.4, 150 mM NaCl, 0.1% NP-40). Lysates were clarified at 21,000 ×
546 *g* for 10 min, and the supernatant was recovered. Equivalent amounts of lysates, as measured
547 by BCA assay (ThermoFisher), were resolved on 4-12% Bis-Tris NuPAGE gels (ThermoFisher),
548 transferred to nitrocellulose, probed with primary and secondary antibodies as noted (see Table)
549 in 5% BSA in TBS-T, and visualized on an Odyssey imaging system (LI-COR, Lincoln NE).
550
551 *Dual-Luciferase Assays*
552 Engineered dCas9-HepG2 cells were seeded into opaque white 96 well plates, at 2.2×10^4 cells
553 per well, in 100 μL growth medium the day prior to transfection. On day of transfection, medium
554 was replaced or changed to sterol-depleted medium (low-glucose DMEM with 5% lipoprotein-
555 deficient serum) with or without 6 μM simvastatin as appropriate. Each well was transfected with
556 100 ng of Luc2-$Prom_{LDLR}$ based construct and 1 ng of secreted nanoluciferase control construct
557 (pSS-NLuc) in a total of 10 μL OptiMEM using Lipofectamine 3000 according to the
558 manufacturer's instructions. 6 replicates were transfected per construct per experiment. After 48
559 hours at 37°C and 5% CO_2, 10 μL of medium was removed from each plate and aliquoted into a
560 separate 384 well plate. Firefly luciferase activity was evaluated in the plates containing the
561 cells by adding an equal volume of a 2× firefly lytic assay buffer (100 mM Tris-HCl pH 7.7, 50
562 mM NaCl, 2 mM $MgCl_2$, 0.17% Triton X-100, 10 mM DTT, 0.4 mM coenzyme A, 0.3 mM ATP,
563 and 0.28 mg/ml luciferin (Goldbio)) *(98)*. Nanoluciferase activity was evaluated from the
564 conditioned medium using a non-lytic 2× coelenterazine (Goldbio) reagent as previously
565 described *(91)*. Raw luminescence was obtained on a SPARK plate reader (Tecan, San Jose
566 CA) with 1 second integration time. Readout of firefly luciferase in each well was normalized to
567 the corresponding secreted nanoluciferase control and data were visually inspected and
568 cleaned to remove values from poorly transfected wells (formally defined by ROUT = 1%) during
569 analysis.
570
571 *Zebrafish Handling, Maintenance, and Cas9-Ribonucleoprotein Knockdowns*
572 All zebrafish studies were performed as previously described*(65)* with minor modifications.
573 Briefly, wild type zebrafish embryos were injected at the one-cell stage with Cas9-RNP
574 complexes and raised at 28 °C. Cas9-RNP complexes were prepared as previously
575 described*(65)* using custom oligonucleotides against the indicated targets (Elim
576 Biopharmaceuticals). Targeting of tyrosinase, which results in larval albinism, was used as an
577 injection control. Larvae were fed a diet of Golden Pearls (5-50 micron, Brine Shrimp Direct,
578 Ogden UT) 3× daily from 4 days post fertilization (dpf), fasted on 7 dpf to clear intestinal
579 cholesterol, and harvested at 8 dpf. Larvae were collected, extensively washed, anesthetized in
580 tricaine, and collected in groups of 10 per sample prior to storage at -80 °C. All zebrafish
581 experiments were performed in accordance with IACUC-approved protocols at the University of
582 California, San Francisco.
583

584 *Cholesterol Analysis of Zebrafish Homogenates*
585 Total cholesterol levels were analyzed as previously described *(66)* with minor modifications.
586 Briefly, frozen larvae were homogenized in PBS with a plastic pestle, and then clarified at
587 18,000 × *g* for 15 min. Supernatants were recovered and total protein content was analyzed by
588 BCA assay. Homogenates were then analyzed, in duplicate, at the appropriate dilution (typically
589 1:12 in PBS) for total cholesterol content using a commercial fluorometric assay (Cayman
590 Chemical, Ann Arbor MI). Fluorescence outputs were measured on a Tecan SPARK plate
591 reader, and cholesterol concentrations were interpolated from a regression line calculated from
592 a standard curve. Cholesterol levels were normalized to total protein content for analysis and
593 subsequently to the scramble control for comparison between experiments.
594
595 *Mouse Handling, Maintenance, and shRNA Knockdowns*
596 All mouse manipulations were performed in accordance with IACUC approved protocols at the
597 University of California, San Francisco following guidelines described in the US National
598 Institutes of Health Guide for the Care and Use of Laboratory Animals. 8-10 week old male
599 C57BL/6 mice (The Jackson Laboratory, Bar Harbor ME) were placed on an atherogenic diet
600 (1.25% cholesterol, 15% fat, 0.5% cholate, D12336i, Research Diets, New Brunswick NJ)*(68)* at
601 the beginning of the experiment (week 0). At week 2, AAV8-packaged shRNA against mouse
602 *Csde1* (NM_144901), *Pcsk9* (NM_153565), or scramble control (Vector Biolabs, Malvern PA)
603 were diluted in sterile PBS to a concentration of 2×10^{11} genomes/ml. 100 µL of diluted AAV8 (2
604 $\times 10^{10}$ genomes/mouse) harboring the appropriate shRNA was administered to each mouse via
605 tail vein injection. At week 4, and again at week 6, mice were fasted overnight and then
606 underwent blood sampling via submandibular vein puncture. Approximately 50 µL of blood was
607 collected into an EDTA-coated tube, centrifuged at 2000 × g for 10 min at 4 ^{o}C, and the plasma
608 recovered and stored at -20 ^{o}C until further analysis. Total cholesterol of the plasma, after
609 approximately 1:200 to 1:400 dilution in assay buffer, was evaluated by commercial fluorometric
610 cholesterol assay (Cayman) as described above. At week 8, mice from the same exposure arm
611 were re-dosed with AAV8 targeting either *Csde1* or scramble control. At week 10, the mice were
612 again fasted overnight and then euthanized after CO_2 narcosis followed by cervical dislocation.
613 The abdominal cavity was opened with a ventral midline incision, the IVC was cannulated, and
614 plasma was collected as described above. The liver and vasculature were perfused with PBS,
615 and the samples of the liver were harvested. Tissue samples for RNA evaluation were placed in
616 TRIzol (ThermoFisher) and those for protein analysis were flash frozen in liquid N_2 and stored at
617 -80 ^{o}C.
618
619 *Lipoprotein Fractionation*
620 Plasma samples were thawed and centrifuged at 2000 × g for 10 min at 4 ^{o}C, and the
621 supernatant recovered. 100 µL of individual mouse plasma was loaded onto a Superose 6
622 Increase 10/300 GL column (Cytiva, Marlborough MA) and eluted with PBS with 1 mM EDTA at
623 0.5 ml/min on an AKTA Pure chromatography system (Cytiva). Fixed 0.5 ml fractions were
624 collected from 0.2 to 1 column volumes along the isocratic elution. Fractions were subjected to
625 total cholesterol analysis and immunoblots as described above.
626
627 *RNA-seq Library Preparation*
628 Total RNA was extracted from frozen liver samples using the Qiagen RNeasy Plus Universal
629 mini kit followed by Manufacturer's instructions (Qiagen). RNA samples were quantified using
630 Qubit 2.0 Fluorometer (ThermoFisher) and RNA integrity was checked using Agilent
631 TapeStation 4200 (Agilent Technologies, Palo Alto CA). Purified RNA was used for mouse
632 qPCR experiments as described above. RNA sequencing libraries were prepared via polyA
633 selection using the NEBNext Ultra RNA Library Prep Kit for Illumina using manufacturer's

instructions (NEB). Briefly, mRNAs were initially enriched with Oligod(T) beads. Enriched mRNAs were fragmented for 15 minutes at 94 °C. First strand and second strand cDNA were subsequently synthesized. cDNA fragments were end repaired and adenylated at 3'ends, and universal adapters were ligated to cDNA fragments, followed by index addition and library enrichment by PCR with limited cycles. The sequencing library was validated on the Agilent TapeStation (Agilent) and quantified by using Qubit 2.0 Fluorometer (Invitrogen) as well as by quantitative PCR (KAPA Biosystems, Wilmington, MA, USA). The sequencing libraries were clustered on a single lane of a flowcell. After clustering, the flowcell was loaded on the Illumina HiSeq instrument (4000 or equivalent) according to manufacturer's instructions. The samples were sequenced using a 2x150bp Paired End (PE) configuration. Image analysis and base calling were conducted by the HiSeq Control Software (HCS). Raw sequence data (.bcl files) generated from Illumina HiSeq was converted into fastq files and de-multiplexed using Illumina's bcl2fastq 2.17 software. One mismatch was allowed for index sequence identification. RNA library preparation and sequencing were conducted by GENEWIZ, LLC (South Plainfield, NJ).

RNA-seq Analysis

All raw sequencing data underwent quality control checks with FastQC (v 0.11.8). Reads were mapped to the mm10 mouse reference genome using Rsubread (v 2.4.3) and assigned to Ensembl gene IDs. Ensemble gene IDs were then mapped to gene symbols using AnnotationDBI (v1.52.0). Gene expression was quantified using raw counts and differential expression gene testing was performed on the scramble-shRNA samples comparing the groups (n=3 in each group) at the highest and lowest levels of raw eGFP expression with EdgeR *(99, 100)* (v.3.32.1) using the glmQLFit method, default settings *(101)*. Statistical significance was set at 5% false discovery rate (FDR; Benjamini-Hochberg). Differential expression gene testing was then performed on the *Csde1*-shRNA and scramble-shRNA at the highest levels of eGFP expression with the overlap of differentially expressed genes identified between these two analyses subsequently removed. Functional enrichment gene-set analysis for GO (Gene Ontology) terms was performed using Enrichr *(102)* via the enrichR R package (v.3.0). Heatmaps were generated using the Bioconductor package ComplexHeatmap *(103)* (v.2.6.2) using log2-transformed CPM values (counts-per-million; values shown are log2-transformed and row-normalized). Volcano plots were generated using the Bioconductor package EnhancedVolcano (v.1.2.0).

Statistical Analysis

Fluorescence values from gated populations in flow cytometry experiments were background corrected by unstained controls and were normalized to the values of the cell line harboring negative control sgRNA. Normalized data were then grouped by the Cochrane method *(104)*, and values for cell lines transduced with individual sgRNAs were compared those of the negative control by T-test with Holm-Sidak correction. For comparison of one-phase decay regression curves in mRNA decay experiments, the extra sum-of-squares F test was used. Pairwise testing to controls was performed in all other experiments using Welch's T-test with Holm-Sidak correction unless otherwise noted. One or two-way ANOVA with Tukey's or Sidak's multiple comparisons tests was used when comparing across all groups in a particular experiment. Adjusted p values < 0.05 were considered significant. Statistical analysis was performed using Prism 7 (GraphPad Software, San Diego CA). All experiments were replicated thrice unless otherwise noted.

Key Resources Tables

Antibodies				
Target	**Fluorophore**	**Clone**	**Source**	**Dilution and Final Conc.**

Human LDL Receptor	Alexa Fluor 647	472413	R&D Systems	1:100, 2 µg/ml (FACS)
Human Transferrin Receptor	Alexa Fluor 647	29806	R&D Systems	1:100, 2 µg/ml (FACS)
Human Transferrin Receptor	Alexa Fluor 488	29806	R&D Systems	1:100, 2 µg/ml (FACS)
Human CSDE1	None	62328	Cell Signaling Technology	1:1000 (WB)
Human beta-Actin	None	8H10D10	Cell Signaling Technology	1:2000 (WB)
Mouse ApoA-I	None	2G4	Santa Cruz Biotechnology	1:1000 (WB)
Mouse ApoB	None	2G11	Millipore Sigma	1:1000 (WB)
Rabbit IgG	IRDye 800CW	926-32211	LI-COR	1:5000, 0.1 µg/ml (WB)
Mouse IgG	IRDye 800CW	926-32210	LI-COR	1:5000, 0.1 µg/ml (WB)

682

qPCR Primers				
Target	**Ref. Sequence**	**Assay ID**	**Source**	**Conc.**
B2M	NM_004048(1)	Hs.PT.58v.18759587	IDT	300 nM
LDLR	NM_000527(6)	Hs.PT.58.2004261	IDT	300 nM
HMGCR	NM_000859(2)	Hs.PT.58.41105492	IDT	300 nM
CSDE1	NM_001007553(6)	Hs.PT.58.40309152	IDT	300 nM
PCSK9	NM_174936(1)	Hs.PT.58.20317141	IDT	300 nM
MYLIP	NM_013262(1)	Hs.PT.58.39124976	IDT	300 nM
TFRC	NM_003234(1)	Hs.PT.39a.22214826	IDT	300 nM
HNRNPD	NM_031369(4)	Hs.PT.58.3757916	IDT	300 nM
KHSRP	NM_003685(1)	Hs.PT.58.555216	IDT	300 nM
B2m	NM_009735(1)	Mm.PT.39a.22214835	IDT	300 nM
Ldlr	NM_001252658(3)	Mm.PT.58.9930556	IDT	300 nM
Csde1	NM_001161854(2)	Mm.PT.58.8160050	IDT	300 nM
eGFP	n/a	Custom Primers Fwd: GAACCGCATCGAGCTGAA Rev: TGCTTGTCGGCCATGATATAG	IDT	300 nM

683

Acknowledgements
We thank Max Horlbeck for guidance with the CRISPRi system, Jonathan D. Brown for helpful discussion on *in vivo* experimental designs, and Paul Cheng and Richard Baylis for helpful discussion on histologic insights and *in vivo* experimental planning. Plasmids for the CRISPRi system were a generous gift from Luke Gilbert and Jonathan Weissman. We thank the Gladstone Institutes Flow Cytometry core facility for their assistance with flow cytometry experiments. UK Biobank analyses were conducted using the UK Biobank resource under application 7089.

Funding Sources
Ar. P. receives support from the Tobacco-Related Disease Research Program (578649), the A.P. Giannini Foundation (P0527061), NIH/NHLBI (K08 HL157700), the Michael Antonov Charitable Foundation Inc., and the Sarnoff Cardiovascular Research Foundation. T.N. is supported by the Japan Society for the Promotion of Science Overseas Research Fellowship. P.N. is supported by a Hassenfeld Scholar Award from the Massachusetts General Hospital, the NIH/NHLBI (R01 HL142711, R01 HL148565, and R01 HL148050), and the Fondation Leducq (TNE-18CVD04). B.L.B. is supported by NIH grants R01 DK119621 and P01 HL146366. D.S. is supported by NIH grants P01 HL098707, P01 HL146366, R01 HL057181 and R01 HL127240, the Roddenberry Foundation, the L.K. Whittier Foundation, the Younger Family Fund, and the NIH/National Center for Research Resources grant C06 RR018928 to the Gladstone Institute. K.M.S. is supported by the Howard Hughes Medical Institute. J.S.C. is supported by the NIH/NHLBI (K08 HL124068 and R03 HL145259), a Pfizer ASPIRE Cardiovascular Award and the Harris Fund and Research Evaluation and Allocation Committee of the UCSF School of Medicine.

Author Contributions
Overall study design: J.S.C. Execution of *in vitro* screen and data processing: G.A.S. Genomic analyses: Ak.P., P.N. *In vitro* validation and synergy experiments, and analysis of mouse blood samples: J.S.C. Execution of zebrafish gene knockdowns: B.H.L., R.S.W. Oversight of zebrafish husbandry: R.S.W., B.L.B. Planning and execution of *in vivo* mouse experiments: Ar.P. Mouse handling, blood, and tissue collection: Ar.P., Y.C.L., T.N., N.S. Processing of RNA-seq data: Ar.P., An.P. Analysis of mouse samples: L.L., R.J. Critical data review and analysis: B.L.B, D.S., K.M.S. Preparation of manuscript: J.S.C. Critical review and revision of manuscript: All authors.

Declaration of Interests
P.N. reports investigator-initiated grant support from Amgen, Apple, and Boston Scientific, and personal fees from Apple, Blackstone Life Sciences, and Novartis, all unrelated to the present work. R.S.W. is an employee of Amgen, Inc. D.S. is the scientific cofounder, shareholder, and director of Tenaya Therapeutics, unrelated to the present work. K.M.S. has consulting agreements for the following companies involving cash and/or stock compensation: Black Diamond Therapeutics, BridGene Bioscences, Denali Therapeutics, Dice Molecules, eFFECTOR Therapeutics, Erasca, Genentech/Roche, Janssen Pharmaceuticals, Kumquat Biosciences, Kura Oncology, Merck, Mitokinin, Petra Pharma, Revolution Medicines, Type6 Therapeutics, Venthera, Wellspring Biosciences (Araxes Pharma). J.S.C. has received consulting fees from Gilde Healthcare and is an unpaid scientific advisor to Eko, both unrelated to this work.

Resource and Data Availability Statement
Additional supporting data are available upon request from the corresponding author. All requests for raw and analyzed data, and materials, including plasmids or cell lines, generated in

735 this study will be responded to promptly. UK Biobank data is available by application to the UK
736 Biobank.
737
738 **Supplementary Materials**
739
740 Figure S1: Validation of dCas9-KRAB-HepG2 Cells.
741 Figure S2: Recovered sgRNAs from Screening Phenotypes.
742 Figure S3: Gene Ontology and Localization Analysis.
743 Figure S4: Selective LDLR Effect of Transmembrane Proteins.
744 Figure S5: Effect of Sterol Conditions on CSDE1 Knockdown.
745 Figure S6: Effect of CSDE1 Overexpression.
746 Figure S7: CSDE1 Knockdown at Protein Level.
747 Figure S8: Effect of *CSDE1* Knockdown on Decay of Non-*LDLR* Transcripts.
748 Figure S9: Physiologic Response of Luciferase Reporter System.
749 Figure S10: Visual Phenotypes of Zebrafish Cas9-sgRNA Saturation Gene Disruption.
750 Figure S11: Effects of *in vivo Csde1* Disruption in Mice.
751
752 Table S1: LDLR Screen Data by Gene *(provided as an Excel file)*
753 Table S2: LDLR Screen Data by Guide *(provided as an Excel file)*
754 Table S3: TFR Screen Data by Gene *(provided as an Excel file)*
755 Table S4: TFR Screen Data by Guide *(provided as an Excel file)*
756 Table S5: LDLR Screen Hits *(provided as an Excel file)*
757 Table S6: TFR Screen Hits *(provided as an Excel file)*
758 Table S7: Baseline Characteristics of UK Biobank Participants in Genomic Association Analyses
759 *(included below)*
760 Table S8: Validation Data by Guide *(provided as an Excel file)*
761 Table S9: Pharmacology Synergy Data by Guide *(provided as an Excel file)*
762 Table S10: Differentially Expressed Genes by *in vivo* RNA Seq *(provided as an Excel file)*
763 Table S11: Enriched GO Terms by *in vivo* RNA Seq *(provided as an Excel file)*
764

References

1. M. S. Brown, J. L. Goldstein, A receptor-mediated pathway for cholesterol homeostasis, *Science (80-.).* (1986), doi:10.1126/science.3513311.

2. J. L. Goldstein, M. S. Brown, A Century of Cholesterol and Coronaries: From Plaques to Genes to Statins, *Cell* **161**, 161–172 (2015).

3. J. L. Goldstein, M. S. Brown, The LDL receptor*Arterioscler. Thromb. Vasc. Biol.* (2009), doi:10.1161/ATVBAHA.108.179564.

4. M. G. Silverman, B. A. Ference, K. Im, S. D. Wiviott, R. P. Giugliano, S. M. Grundy, E. Braunwald, M. S. Sabatine, Association Between Lowering LDL-C and Cardiovascular Risk Reduction Among Different Therapeutic Interventions, *JAMA* **316**, 1289 (2016).

5. K. D. Kochanek, J. Xu, E. Arias, Mortality in the United States, 2019., *NCHS Data Brief* , 1–8 (2020).

6. G. G. Schwartz, P. G. Steg, M. Szarek, D. L. Bhatt, V. A. Bittner, R. Diaz, J. M. Edelberg, S. G. Goodman, C. Hanotin, R. A. Harrington, J. W. Jukema, G. Lecorps, K. W. Mahaffey, A. Moryusef, R. Pordy, K. Quintero, M. T. Roe, W. J. Sasiela, J. F. Tamby, P. Tricoci, H. D. White, A. M. Zeiher, L. B. Schiavi, M. Garrido, A. F. Alvarisqueta, S. A. Sassone, A. P. Bordonava, A. E. Alves De Lima, J. M. Schmidberg, E. A. Duronto, O. C. Caruso, L. P. Novaretto, M. A. Hominal, O. R. Montaña, A. Caccavo, O. A. Gomez Vilamajo, A. J. Lorenzatti, L. R. Cartasegna, G. A. Paterlini, I. J. Mackinnon, G. D. Caime, M. Amuchastegui, O. R. Codutti, H. O. Jure, J. O. E. Bono, A. D. Hrabar, J. A. Vallejos, R. A. Ahuad Guerrero, F. Novoa, C. A. Patocchi, C. J. Zaidman, M. E. Giuliano, R. D. Dran, M. L. Vico, G. S. Carnero, P. N. Guzman, J. C. Medrano Allende, D. F. Garcia Brasca, M. H. Bustamante Labarta, S. Nani, E. D. S. Blumberg, H. R. Colombo, A. Liberman, H. L. Luciardi, G. D. Waisman, M. A. Berli, R. O. Garcia Duran, H. G. Cestari, H. A. Luquez, J. A. Giordano, S. S. Saavedra, J. H. Waites, N. Collins, A. Soward, P. E. Aylward, C. L. S. Hii, J. Shaw, M. A. Arstall, J. Horowitz, J. F. Rogers, D. Colquhoun, R. E. Oqueli Flores, P. Roberts-Thomson, O. Raffel, S. J. Lehman, S. G. M. Coverdale, P. J. Garrahy, G. Starmer, M. Sader, P. A. Carroll, R. Zweiker, U. Hoppe, H. Drexel, K. Huber, R. Berger, F. Weidinger, D. Faes, K. Hermans, B. Pirenne, A. Leone, E. Hoffer, P. Sinnaeve, M. C. M. Vrolix, L. De Wolf, B. Wollaert, M. Castadot, K. Dujardin, C. Beauloye, G. Vervoort, H. Striekwold, C. Convens, J. Roosen, E. Barbato, M. Claeys, F. Cools, I. Terzic, F. Barakovic, Z. Midzic, B. Pojskic, E. Fazlibegovic, M. Dilic, A. Durak-Nalbantic, D. Vulic, A. Muslibegovic, G. Reis, L. Sousa, J. C. Nicolau, F. E. Giorgeto, R. P. Silva, L. Nigro Maia, R. Rech, P. R. F. Rossi, M. Cerqueira, N. Duda, R. Kalil, A. Kormann, J. A. M. Abrantes, P. Pimentel Filho, A. P. Soggia, M. O. N. de Santos, F. Neuenschwander, L. C. Bodanese, Y. L. Michalaros, F. G. Eliaschewitz, M. H. Vidotti, P. E. Leaes, R. V. Botelho, S. Kaiser, E. R. F. Fernandes Manenti, D. B. Precoma, J. C. Moura Jorge, P. G. M. de B Silva, J. A. Silveira, W. Saporito, J. A. Marin Neto, G. S. Feitosa, L. E. F Ritt, J. A. de Souza, F. Costa, W. Souza, H. J. L. Reis, R. D. Lopes, L. Machado, J. C. Aidar Ayoub, G. V. Todorov, F. P. Nikolov, E. S. Velcheva, M. L. Tzekova, H. O. Benov, S. L. Petranov, H. S. Tumbev, N. S. Shehova-Yankova, D. T. Markov, D. H. Raev, M. N. Mollov, K. N. Kichukov, K. A. Ilieva-Pandeva, N. N. Gotcheva, R. Ivanova, V. M. Mincheva, P. V. Lazov, B. I. Dimov, M. Senaratne, J. Stone, J. Kornder, S. Pearce, D. Dion, D. Savard, Y. Pesant, A. Pandey, S. Robinson, G. Gosselin, S. Vizel, G. Hoag, R. Bourgeois, A. Morisset, E. Sabbah, B. Sussex, S. Kouz, P. MacDonald, N. Michaud, D. Fell, R. Leung, T. Vuurmans, C. Lai, F. Nigro, R. Davies, G. Nogareda, R. Vijayaraghavan, J. Ducas, S. Lepage, S. Mehta, J. Cha, R. Dupuis, P. Fong, J. Rodes-Cabau, H. Fadlallah, D. Cleveland, T. Huynh, I. Bata, A. Hameed, C. Pincetti, S. Potthoff, J. C. Prieto, M. Acevedo, A. Aguirre, M. Vejar, M. Yañez, G. Araneda, M. Fernandez, L. Perez, P. Varleta, F. Florenzano, L. Huidobro, C. A. Raffo, C. Olivares, J. Chen, Y. Dong, W. Huang, J. Wang, S. Huang, Z. Yao, L. Cui, W. Lin, Y. Sun, J. Li, X. Zhang, H. Zhu, D. Chen, L. Huang, S. Dong, G. Su, B. Xu, X. Su, X. Cheng, J. Lin, W. Zong, H. Li, Y. Feng, D. Xu, X. Yang, Y. Ke, X. Lin, Z. Zhang, Z. Zheng, Z. Luo, Y. Chen, C. Ding, Y. Zheng, X. Li, D. Peng, Y. Li, M. Wei, S. Liu, Y. Yu, B. Qu, W. Jiang, Y. Zhou, X. Zhao, Z. Yuan, Y. Guo, X. Xu,

X. Shi, J. Ge, G. Fu, F. Bai, W. Fang, X. Shou, N. Jaramillo, G. Sanchez Vallejo, D. C. Luna Botia, R. Botero Lopez, D. I. Molina De Salazar, A. J. Cadena Bonfanti, J. Diego Higuera, S. I. Barrera Silva, H. J. Garcia Lozada, J. A. Coronel Arroyo, J. L. Accini Mendoza, R. L. Fernandez Ruiz, A. M. Fernandez, F. G. Manzur Jatin, A. Sotomayor Herazo, J. Castellanos Parada, M. A. Urina Triana, M. Strozzi, S. Car, D. Miličić, M. L. Benčić, H. Pintarić, D. Prvulović, J. Šikić, V. Peršić, D. Mileta, K. Štambuk, Z. Babić, J. Spinar, D. Horak, J. Stasek, D. Alan, V. Machova, A. Linhart, V. Novotny, V. Kaucak, R. Rokyta, R. Naplava, Z. Coufal, V. Adamkova, I. Podpera, J. Zizka, Z. Motovska, I. Marusincova, P. Svab, P. Ostadal, P. Heinc, J. Kuchar, P. Povolny, S. H. Poulsen, B. Raungaard, P. Clemmensen, L. E. Bang, O. May, M. Bøttcher, J. D. Hove, L. Frost, G. Gislason, J. Larsen, P. B. Johansen, F. Hald, J. Jeppesen, T. Nielsen, K. S. Kristensen, P. M. Walichiewicz, J. D. Lomholdt, I. C. Klausen, P. K. Nielsen, F. Davidsen, L. Videbaek, M. Viigimaa, M. Soots, V. Vahula, A. Hedman, U. Soopõld, K. Märtsin, M. R. Taskinen, K. Porthan, J. K. Airaksinen, M. Juonala, T. Kiviniemi, S. Vikman, P. Posio, J. Taurio, H. Huikuri, K. Kaikkonen, P. Coste, E. Ferrari, N. Danchin, O. Morel, G. Montalescot, G. Barone-Rochette, J. Mansourati, Y. Cottin, F. Leclercq, A. Belhassane, N. Delarche, F. Boccara, F. Paganelli, J. Clerc, F. Schiele, V. Aboyans, V. Probst, J. Berland, T. Lefèvre, V. Chumburidze, I. Khintibidze, T. Shaburishvili, Z. Pagava, R. Ghlonti, Z. Lominadze, G. Khabeishvili, R. Hemetsberger, U. Rauch-Kröhnert, M. Stratmann, K. F. Appel, E. Schmidt, H. Omran, C. Stellbrink, T. Dorsel, E. Lianopoulos, R. Marx, A. Zirlik, D. Schellenberg, T. Heitzer, U. Laufs, N. Marx, S. Gielen, B. Winkelmann, S. Behrens, K. Sydow, G. Simonis, T. Muenzel, N. Werner, S. Leggewie, D. Böcker, R. Braun-Dullaeus, N. Toursarkissian, M. Jeserich, M. Weißbrodt, T. Schaeufele, J. Weil, H. Völler, J. Waltenberger, M. Natour, S. Steiner, L. Heidenreich, U. Gremmler, H. Killat, S. Patsilinakos, A. Kartalis, A. Manolis, D. Sionis, E. Liberopoulos, I. Skoumas, V. Athyros, P. Vardas, F. Parthenakis, D. Alexopoulos, G. Hahalis, J. Lekakis, A. Xatzitolios, S. R. Fausto Ovando, P. C. Montenegro Valdovinos, J. L. Arango Benecke, E. R. Rodriguez De Leon, B. P. Y. Yan, D. C. W. Siu, T. Turi, B. Merkely, R. G. Kiss, I. Ungi, G. Lupkovics, L. Nagy, A. Katona, I. Édes, G. Müller, I. Horvath, T. Kapin, J. Faluközy, M. Kumbla, M. Sandhu, S. Annam, N. R. Proddutur, R. K. Premchand, A. Mahajan, A. D. Abhyanakar, P. Kerkar, R. A. Govinda, A. Oomman, D. Sinha, S. N. Patil, D. Kahali, J. Sawhney, A. B. Joshi, S. Chaudhary, P. Harkut, S. Guha, S. Porwal, S. Jujjuru, R. B. Pothineni, M. R. Monteiro, A. Khan, S. S. Iyengar, J. S. Grewal, M. Chopda, M. C. Fulwani, A. Patange, V. K. Chopra, N. K. Goyal, R. Shinde, G. V. Manakshe, N. Patki, S. Sethi, V. Munusamy, S. Karna, S. Adhyapak, U. Pandurangi, R. Mathur, S. Kalashetti, A. Bhagwat, B. Raghuraman, S. K. Yerra, P. Bhansali, R. Borse, S. Das, J. Abdullakutty, S. Saathe, P. Palimkar, S. Atar, M. Shechter, M. Mosseri, Y. Arbel, C. Lotan, U. Rosenschein, A. Katz, Y. Henkin, A. Francis, M. Klutstein, E. Nikolsky, Y. Turgeman, M. Halabi, R. Kornowski, M. Jonas, O. Amir, Y. Rozenman, S. Fuchs, O. Hussein, D. Gavish, Z. Vered, Y. Caraco, M. Elias, N. Tov, G. Piovaccari, A. De Pellegrin, G. Guardigli, G. Licciardello, C. Auguadro, C. Cuccia, A. Salvioni, G. Musumeci, P. Calabrò, S. Novo, P. Faggiano, N. B. De Cesare, S. Berti, C. Cavallini, E. Puccioni, M. Galvani, M. Tespili, P. Piatti, M. Palvarini, G. De Luca, R. Violini, A. De Leo, P. Perrone Filardi, M. Ferratini, K. Dai, H. Kamiya, K. Ando, Y. Takeda, Y. Morino, Y. Hata, K. Kimura, K. Kishi, I. Michishita, H. Uehara, T. Higashikata, A. Hirayama, K. Hirooka, S. Sakagami, S. Taguchi, A. Koike, H. Fujinaga, S. Koba, K. Kozuma, T. Kawasaki, Y. Ono, M. Shimizu, Y. Katsuda, A. Wada, T. Shinke, T. Kimura, J. Ako, K. Fujii, T. Takahashi, T. Sakamoto, Y. Furukawa, H. Sugino, T. Mano, N. Utsu, K. Ito, T. Haraguchi, Y. Ueda, A. Nishibe, K. Fujimoto, J. H. Yoon, S. H. Kim, H. S. Park, I. H. Chae, M. H. Kim, M. H. Jeong, S. Rha, C. Kim, H. S. Kim, T. Hong, A. Busmane, N. Pontaga, A. Strelnieks, I. Mintale, I. Sime, Z. Petrulioniene, R. Kavaliauskiene, R. Jurgaitiene, G. Sakalyte, R. Slapikas, S. Norkiene, N. Misonis, A. Kibarskis, R. Kubilius, S. Bojovski, S. Kedev, N. Lozance, A. Kjovkaroski, S. Doncovska, T. K. Ong, S. Kasim, O. Maskon, B. Kandasamy, K. Yusoff, H. B. Liew, W. M. I. Wan Mohamed, A. García Castillo, G. A. Ramos López, J. Carrillo Calvillo, P. Fajardo Campos, J. C. Núñez Fragoso, E. A. Bayram Llamas, M. A. Alcocer Gamba, J. Carranza Madrigal, L. G.

González Salas, E. López Rosas, B. González Díaz, E. Salcido Vázquez, A. Nacoud Ackar, G. A. Llamas Esperón, C. R. Martínez Sánchez, M. Guerrero De Leon, R. Suarez Otero, G. Fanghänel Salmón, J. A. Pérez Ríos, J. A. Garza Ruíz, M. Alings, R. W. Breedveld, P. A. M. Hoogslag, H. Suryapranata, A. Oomen, J. J. Wiersma, R. M. A. Van Der Wal, P. S. Hooft Van Huysduynen-Monraats, I. Karalis, G. J. E. Verdel, B. R. G. Brueren, R. P. T. Troquay, E. P. Viergever, N. Y. Y. Al-Windy, G. L. Bartels, J. H. Cornel, W. R. M. Hermans, J. P. R. Herrman, R. J. Bos, R. Groutars, C. C. Van Der Zwaan, R. Kaplan, E. Ronner, B. E. Groenemeijer, P. N. A. Bronzwaer, A. A. H. Liem, B. Rensing, M. Bokern, R. Nijmeijer, F. Hersbach, F. F. Willems, A. T. M. Gosselink, J. Elliott, G. Wilkins, R. Fisher, D. Scott, H. Hart, R. Stewart, S. Harding, I. Ternouth, N. Fisher, D. Aitken, R. Anscombe, T. Tomala, O. Nygård, J. A. Sparby, K. Andersen, L. Gullestad, J. Jortveit, P. S. Munk, S. Halvorsen, U. Hurtig, R. M. Correa Flores, J. R. Calderon Ticona, J. R. Durand Velasquez, S. A. Negron Miguel, E. S. Sanabria Perez, J. M. Carrion Chambilla, C. A. Chavez Ayala, R. P. Castillo Leon, R. J. Vargas Gonzales, J. D. Hernandez Zuniga, L. A. Camacho Cosavalente, J. E. Bravo Mannucci, N. C. Llerena Navarro, Y. M. Roldan Concha, V. E. Rodriguez Chavez, H. A. Anchante Hernandez, C. A. Zea Nunez, A. Ferrolino, R. A. G. Sy, L. Tirador, R. G. Sy, G. Matiga, R. M. Coching, A. Bernan, G. Rogelio, D. D. Morales, E. Tan, A. Wlodarczak, K. Jaworska, G. Skonieczny, L. Pawlowicz, P. Wojewoda, B. Busz-Papiez, J. Bednarski, A. Goch, P. Staneta, E. Dulak, A. Budaj, K. Saminski, W. Krasowski, W. Sudnik, A. Zurakowski, M. Skorski, R. Lysek, B. Miklaszewicz, J. Kubica, J. A. Lipko, E. Kostarska-Srokosz, M. Piepiorka, A. Drzewiecka, R. Sciborski, A. Stasiewski, T. Blicharski, L. Bystryk, M. Szpajer, M. Korol, T. Czerski, E. Mirek-Bryniarska, J. Gniot, A. Lubinski, J. Gorny, E. Franek, P. Monteiro, J. Mesquita Bastos, H. H. Pereira, D. Martins, J. Morais, F. Seixo, C. Mendonça, A. Botelho, B. Minescu, O. Istratoaie, D. N. Tesloianu, M. Dorobantu, G. Cristian, C. G. C. Podoleanu, M. C. A. Constantinescu, C. M. Bengus, C. Militaru, D. Rosu, I. R. Parepa, A. V. Matei, T. M. Alexandru, Y. Shvarts, O. Orlikova, Z. Kobalava, O. L. Barbarash, V. Markov, N. Lyamina, A. Gordienko, K. Zrazhevsky, A. Y. Vishnevsky, V. Gurevich, R. Stryuk, N. V. Lomakin, I. Bokarev, S. Shalaev, L. Khaisheva, P. Chizhov, I. Viktorova, N. Osokina, E. Akatova, G. Chumakova, I. Libov, M. I. Voevoda, T. V. Tretyakova, E. Baranov, S. Shustov, S. Yakushin, I. Gordeev, N. Khasanov, O. Reshetko, T. Sotnikova, O. Molchanova, K. Y. Nikolaev, L. Gapon, E. Baranova, Z. Shogenov, E. Kosmachova, Y. Karpov, A. Povzun, L. Egorova, V. V. Tyrenko, I. G. Ivanov, D. Simic, N. Ivanovic, G. Davidovic, N. Tasic, M. R. Asanin, S. Stojic, S. R. Apostolovic, S. Ilic, B. Putnikovic, A. Stankovic, A. Arandjelovic, S. Radovanovic, A. D. Ristic, J. Balinovac, D. V. Dincic, P. Seferovic, S. Dodic, S. Dimkovic, T. Chua, K. K. Poh, H. Y. Ong, K. Micko, J. Nociar, D. Pella, P. Fulop, M. Hranai, J. Palka, J. Mazur, I. Majercák, A. Dzupina, F. Fazekas, J. Gonsorcik, V. Bugan, J. Murin, J. Selecky, G. Kamensky, J. Strbova, R. Smik, A. Dukat, I. Žuran, J. Oklukar, N. C. Šuligoj, M. Cevc, L. Lipar, H. P. Cyster, N. Ranjith, C. Corbett, J. Bayat, E. M. Makotoko, I. E. Kapp, M. M. V. Basson, H. Lottering, L. J. Van Zyl, P. J. Sebastian, T. Pillay, J. A. Saaiman, P. J. Commerford, S. Cassimjee, I. O. Ebrahim, M. Sarvan, J. H. Mynhardt, A. J. Dalby, H. Reuter, R. Moodley, M. Vida, A. R. Cequier Fillat, V. Bodí Peris, F. Fuentes Jimenez, F. Marín, J. M. Cruz Fernández, B. Gil-Extremera, F. W. Diz, D. Garcia-Dorado, A. Iñiguez, J. Tuñón Fernández, J. R. Gonzalez-Juanatey, J. Fernandez Portales, F. Civeira Murillo, L. Matas Pericas, J. L. Zamorano, M. De Mora Martin, J. Bruguera Cortada, J. J. Alonso Martin, J. R. De Berrazueta Fernández, J. F. Díaz Fernández, J. A. García Lledó, J. Cosín Sales, J. Botas Rodriguez, G. Gusi Tragant, A. Benedicto, C. Gonzalez-Juanatey, M. Camprubí Potau, I. Plaza Perez, C. M. De La Tassa, P. Loma-Osorio Rincon, J. Balaguer Recena, J. M. Escudier, G. Constantine, R. Haniffa, N. Tissera, S. Amarasekera, N. Fernando, J. Jayawardena, W. Santharaj, R. Ekanayaka, S. Mendis, V. Senaratne, G. Mayurathan, T. Sirisena, A. Rajapaksha, J. I. Herath, N. Amarasena, S. Berglund, G. Rasmanis, E. Hagström, N. Witt, G. Mourtzinis, P. Nicol, O. Hansen, S. Romeo, S. A. Jensen, I. Torstensson, U. Ahremark, T. Sundelin, T. Moccetti, C. Müller, F. Mach, R. Binder, C. E. Chiang, W. C. Tsai, K. C. Ueng, W. T. Lai, M. E. Liu, J. J.

Hwang, W. H. Yin, I. C. Hsieh, W. H. Lin, J. Y. Kuo, T. Y. Huang, C. Y. Fang, P. Kaewsuwanna, W. Soonfuang, W. Jintapakorn, A. Sukonthasarn, P. Sritara, N. Wongpraparut, K. Sastravaha, N. Sansanayudh, W. Kehasukcharoen, D. Piyayotai, A. Camsari, H. Kultursay, S. Guneri, B. Mutlu, M. Ersanli, M. Demirtas, C. Kirma, E. Ural, L. Koldas, O. Karpenko, A. Prokhorov, I. Vakaluyk, H. Myshanych, D. Reshotko, V. Batushkin, L. Rudenko, I. Kovalskyi, M. Kushnir, V. Tseluyko, Y. Mostovoy, M. Stanislavchuk, Y. Kyiak, Y. Karpenko, Y. Malynovsky, A. Klantsa, O. Kutniy, E. Amosova, V. Tashchuk, O. Leshchuk, A. Parkhomenko, M. Rishko, M. Kopytsya, A. Yagensky, M. Vatutin, A. Bagriy, O. M. Barna, O. Ushakov, G. Dzyak, B. Goloborodko, A. Rudenko, J. Trevelyan, A. Zaman, K. Lee, A. Moriarty, R. K. Aggarwal, P. Clifford, Y. K. Wong, S. M. R. Iqbal, E. Subkovas, D. Braganza, D. Sarkar, R. Storey, H. Griffiths, S. Mcclure, R. Muthusamy, J. Kurian, T. Levy, C. Barr, H. Kadr, R. Gerber, A. Simaitis, H. Soran, A. Mathur, A. Brodison, R. Oliver, T. Mudawi, T. Reynolds, D. Sharman, R. Butler, P. Wilkinson, G. Y. H. Lip, J. Halcox, G. Vardi, D. Baldari, D. Brabham, C. Treasure, C. Dahl, B. Palmer, A. Wiseman, S. Puri, A. E. Mohart, C. Ince, E. Flores, S. Wright, S. C. Cheng, M. Rosenberg, W. Rogers, E. Kosinski, L. Forgosh, J. Waltman, M. Khan, M. Shoukfeh, G. Dagher, I. Lieber, P. Kumar, C. East, P. Krichmar, L. White, T. Knickelbine, T. Haldis, E. Gillespie, D. Suh, I. Arif, F. Akhter, E. Carlson, M. D'Urso, F. El-Ahdab, W. Nelson, B. Harris, S. Cohen, L. Carter, K. Sabatino, T. Haddad, A. Malik, S. Rao, A. Mulkay, I. Jovin, K. Klancke, V. Malhotra, S. K. Devarapalli, M. Koren, H. Chandna, G. Dodds, M. Janik, J. Moran, A. Sumner, J. Kobayashi, W. Davis, S. Yazdani, J. Pasquini, M. Thakkar, A. Vedere, W. Leimbach, J. Rider, N. Singh, A. V. Shah, P. M. Moriarty, D. Janosik, C. Pepine, B. Berman, J. Gelormini, C. Daniels, F. Keating, N. I. Kondo, S. Shetty, W. Waider, T. Takata, M. Abu-Fadel, V. Shah, R. Aggarwal, M. Izzo, A. Kumar, B. Hattler, C. Link, A. Bortnick, G. Kinzfogl, A. Ghitis, J. Larry, E. Teufel, P. Kuhlman, B. Mclaurin, W. Zhang, S. Thew, J. Abbas, M. White, N. Ranadive, C. Gring, D. Henderson, T. Schuchard, N. Farhat, G. Kline, S. Mahal, J. Whitaker, S. Speirs, R. Andersen, N. Daboul, P. Horwitz, Z. Jafar, J. Mcgarvey, V. Panchal, S. Voyce, T. Blok, W. Sheldon, M. M. Azizad, C. Schmalfuss, M. Picone, W. Herzog, J. Lindsey, R. Nowins, N. Lepor, M. El Shahawy, H. Weintraub, A. Irimpen, W. May, T. Galski, A. Chu, F. Mody, Z. Hodes, J. Fairlamb, C. Lambert, A. Raisinghani, A. Abbate, M. King, C. Carey, J. Gerber, L. Younis, H. T. Park, M. Vidovich, T. Knutson, D. Friedman, F. Chaleff, A. Loussararian, C. Kimmelstiel, K. Silver, M. Foster, G. Tonnessen, M. Amlani, A. Wali, C. Malozzi, K. Wattanakit, P. J. O'Donnell, D. Singal, N. Jaffrani, S. Banuru, D. Fisher, M. Xenakis, N. Perlmutter, R. Bhagwat, J. Strader, A. Akyea-Djamson, A. Labroo, H. J. Marais, E. Claxton, M. Berk, P. Rossi, P. Joshi, A. S. Khaira, G. Kumkumian, S. Lupovitch, J. Purow, S. Welka, D. Hoffman, S. Fischer, E. Soroka, D. Eagerton, S. Pancholy, M. Ray, M. Farrar, S. Pollock, W. J. French, S. Diamantis, L. Gimple, S. Schwartz, E. Pereira, D. Spriggs, J. Strain, A. Vo, M. Chane, J. Hall, N. Vijay, K. Lotun, F. M. Lester, A. Nahhas, T. Pope, P. Nager, R. Vohra, R. Bashir, H. Ahmed, M. Berlowitz, R. Fishberg, R. Barrucco, E. Yang, M. Radin, D. Sporn, S. Eisenberg, J. Landzberg, M. Mcgough, S. Turk, M. Schwartz, P. S. Sundram, D. Jain, M. Zainea, C. Bayron, R. Karlsberg, H. Lui, W. Keen, D. Westerhausen, S. Khurana, H. Agarwal, J. Birchem, W. Penny, M. Chang, J. M. Gilbert, G. Chalavarya, C. Eaton, J. F. Schmedtje, S. Christenson, D. Denham, A. Macdonell, P. Gibson, A. Rahman, T. Al Joundi, G. Conrad, P. Kotha, M. Love, G. Giesler, H. Rubenstein, L. Akright, B. Schifferdecker, J. Krawczyk, T. Wells, J. Welker, R. Foster, R. Gilmore, J. Anderson, D. Jacoby, G. Gardner, R. Dandillaya, K. Vora, J. Kostis, J. Hunter, D. Laxson, E. Ball, Alirocumab and cardiovascular outcomes after acute coronary syndrome, *N. Engl. J. Med.* (2018), doi:10.1056/NEJMoa1801174.

7. M. S. Sabatine, R. P. Giugliano, A. C. Keech, N. Honarpour, S. D. Wiviott, S. A. Murphy, J. F. Kuder, H. Wang, T. Liu, S. M. Wasserman, P. S. Sever, T. R. Pedersen, FOURIER Steering Committee and Investigators, Evolocumab and Clinical Outcomes in Patients with Cardiovascular Disease, *N. Engl. J. Med.* **376**, 1713–1722 (2017).

8. C. Ma, M. E. Gurol, Z. Huang, A. H. Lichtenstein, X. Wang, Y. Wang, S. Neumann, S. Wu, X.

969 Gao, Low-density lipoprotein cholesterol and risk of intracerebral hemorrhage, *Neurology*
970 (2019), doi:10.1212/WNL.0000000000007853.
971 9. M. S. Sabatine, S. D. Wiviott, K. Im, S. A. Murphy, R. P. Giugliano, Efficacy and safety of
972 further lowering of low-density lipoprotein cholesterol in patients starting with very low levels: A
973 meta-analysis, *JAMA Cardiol.* (2018), doi:10.1001/jamacardio.2018.2258.
974 10. R. P. Giugliano, T. R. Pedersen, J.-G. Park, G. M. De Ferrari, Z. A. Gaciong, R. Ceska, K.
975 Toth, I. Gouni-Berthold, J. Lopez-Miranda, F. Schiele, F. Mach, B. R. Ott, E. Kanevsky, A. L.
976 Pineda, R. Somaratne, S. M. Wasserman, A. C. Keech, P. S. Sever, M. S. Sabatine, FOURIER
977 Investigators, Clinical efficacy and safety of achieving very low LDL-cholesterol concentrations
978 with the PCSK9 inhibitor evolocumab: a prespecified secondary analysis of the FOURIER trial,
979 *Lancet* **390**, 1962–1971 (2017).
980 11. A. Taylor, D. Wang, K. Patel, R. Whittall, G. Wood, M. Farrer, R. D. Neely, S. Fairgrieve, D.
981 Nair, M. Barbir, J. L. Jones, S. Egan, R. Everdale, Y. Lolin, E. Hughes, J. A. Cooper, S. G.
982 Hadfield, G. Norbury, S. E. Humphries, Mutation detection rate and spectrum in familial
983 hypercholesterolaemia patients in the UK pilot cascade project, *Clin. Genet.* **77**, 572–580
984 (2010).
985 12. A. Garg, S. Fazio, P. B. Duell, A. Baass, C. Udata, T. Joh, T. Riel, M. Sirota, D. Dettling, H.
986 Liang, P. D. Garzone, B. Gumbiner, H. Wan, Molecular Characterization of Familial
987 Hypercholesterolemia in a North American Cohort, *J. Endocr. Soc.* (2019),
988 doi:10.1210/jendso/bvz015.
989 13. L. A. Gilbert, M. A. Horlbeck, B. Adamson, J. E. Villalta, Y. Chen, E. H. Whitehead, C.
990 Guimaraes, B. Panning, H. L. Ploegh, M. C. Bassik, L. S. Qi, M. Kampmann, J. S. Weissman,
991 Genome-Scale CRISPR-Mediated Control of Gene Repression and Activation, *Cell* **159**, 647–
992 661 (2014).
993 14. M. A. Horlbeck, L. A. Gilbert, J. E. Villalta, B. Adamson, R. A. Pak, Y. Chen, A. P. Fields, C.
994 Y. Park, J. E. Corn, M. Kampmann, J. S. Weissman, Compact and highly active next-generation
995 libraries for CRISPR-mediated gene repression and activation., *Elife* **5** (2016),
996 doi:10.7554/eLife.19760.
997 15. B. Adamson, T. M. Norman, M. Jost, M. Y. Cho, J. K. Nuñez, Y. Chen, J. E. Villalta, L. A.
998 Gilbert, M. A. Horlbeck, M. Y. Hein, R. A. Pak, A. N. Gray, C. A. Gross, A. Dixit, O. Parnas, A.
999 Regev, J. S. Weissman, A Multiplexed Single-Cell CRISPR Screening Platform Enables
1000 Systematic Dissection of the Unfolded Protein Response., *Cell* **167**, 1867-1882.e21 (2016).
1001 16. K. K. Ray, R. S. Wright, D. Kallend, W. Koenig, L. A. Leiter, F. J. Raal, J. A. Bisch, T.
1002 Richardson, M. Jaros, P. L. J. Wijngaard, J. J. P. Kastelein, Two phase 3 trials of inclisiran in
1003 patients with elevated LDL cholesterol, *N. Engl. J. Med.* (2020), doi:10.1056/NEJMoa1912387.
1004 17. B. B. Knowles, C. C. Howe, D. P. Aden, Human hepatocellular carcinoma cell lines secrete
1005 the major plasma proteins and hepatitis B surface antigen, *Science (80-.).* (1980),
1006 doi:10.1126/science.6248960.
1007 18. M. A. Mandegar, N. Huebsch, E. B. Frolov, E. Shin, A. Truong, M. P. Olvera, A. H. Chan, Y.
1008 Miyaoka, K. Holmes, C. I. Spencer, L. M. Judge, D. E. Gordon, T. V. Eskildsen, J. E. Villalta, M.
1009 A. Horlbeck, L. A. Gilbert, N. J. Krogan, S. P. Sheikh, J. S. Weissman, L. S. Qi, P. L. So, B. R.
1010 Conklin, CRISPR Interference Efficiently Induces Specific and Reversible Gene Silencing in
1011 Human iPSCs, *Cell Stem Cell* (2016), doi:10.1016/j.stem.2016.01.022.
1012 19. A. W. Alberts, J. Chen, G. Kuron, V. Hunt, J. Huff, C. Hoffman, J. Rothrock, M. Lopez, H.
1013 Joshua, E. Harris, A. Patchett, R. Monaghan, S. Currie, E. Stapley, G. Albers-Schonberg, O.
1014 Hensens, J. Hirshfield, K. Hoogsteen, J. Liesch, J. Springer, Mevinolin: A highly potent
1015 competitive inhibitor of hydroxymethylglutaryl-coenzyme A reductase and a cholesterol-lowering
1016 agent, *Proc. Natl. Acad. Sci. U. S. A.* (1980), doi:10.1073/pnas.77.7.3957.
1017 20. M. S. Brown, J. R. Faust, J. L. Goldstein, I. Kaneko, A. Endo, Induction of 3-hydroxy-3-
1018 methylglutaryl coenzyme A reductase activity in human fibroblasts incubated with compactin
1019 (ML-236B), a competitive inhibitor of the reductase, *J. Biol. Chem.* (1978).

1020 21. S. Benjannet, D. Rhainds, R. Essalmani, J. Mayne, L. Wickham, W. Jin, M.-C. Asselin, J.
1021 Hamelin, M. Varret, D. Allard, M. Trillard, M. Abifadel, A. Tebon, A. D. Attie, D. J. Rader, C.
1022 Boileau, L. Brissette, M. Chrétien, A. Prat, N. G. Seidah, NARC-1/PCSK9 and its natural
1023 mutants: zymogen cleavage and effects on the low density lipoprotein (LDL) receptor and LDL
1024 cholesterol., *J. Biol. Chem.* **279**, 48865–75 (2004).
1025 22. S. Rashid, D. E. Curtis, R. Garuti, N. N. Anderson, Y. Bashmakov, Y. K. Ho, R. E. Hammer,
1026 Y. A. Moon, J. D. Horton, Decreased plasma cholesterol and hypersensitivity to statins in mice
1027 lacking Pcsk9, *Proc. Natl. Acad. Sci. U. S. A.* **102**, 5374–5379 (2005).
1028 23. J. C. Chan, D. E. Piper, Q. Cao, D. Liu, C. King, W. Wang, J. Tang, Q. Liu, J. Higbee, Z. Xia,
1029 Y. Di, S. Shetterly, Z. Arimura, H. Salomonis, W. G. Romanow, S. T. Thibault, R. Zhang, P.
1030 Cao, X. P. Yang, T. Yu, M. Lu, M. W. Retter, G. Kwon, K. Henne, O. Pan, M. M. Tsai, B.
1031 Fuchslocher, E. Yang, L. Zhou, K. J. Lee, M. Daris, J. Sheng, Y. Wang, W. D. Shen, W. C. Yeh,
1032 M. Emery, N. P. Walker, B. Shan, M. Schwarz, S. M. Jackson, A proprotein convertase
1033 subtilisin/kexin type 9 neutralizing antibody reduces serum cholesterol in mice and nonhuman
1034 primates, *Proc. Natl. Acad. Sci. U. S. A.* **106**, 9820–9825 (2009).
1035 24. P. Aisen, Transferrin receptor 1., *Int. J. Biochem. Cell Biol.* **36**, 2137–43 (2004).
1036 25. R. Coffey, T. Ganz, Iron homeostasis: An anthropocentric perspective, *J. Biol. Chem.* **292**,
1037 12727–12734 (2017).
1038 26. N. Zelcer, C. Hong, R. Boyadjian, P. Tontonoz, LXR regulates cholesterol uptake through
1039 Idol-dependent ubiquitination of the LDL receptor, *Science* **325**, 100–104 (2009).
1040 27. M. Yoshinaga, Y. Nakatsuka, A. Vandenbon, D. Ori, T. Uehata, T. Tsujimura, Y. Suzuki, T.
1041 Mino, O. Takeuchi, Regnase-1 Maintains Iron Homeostasis via the Degradation of Transferrin
1042 Receptor 1 and Prolyl-Hydroxylase-Domain-Containing Protein 3 mRNAs, *Cell Rep.* (2017),
1043 doi:10.1016/j.celrep.2017.05.009.
1044 28. H. Mi, A. Muruganujan, D. Ebert, X. Huang, P. D. Thomas, PANTHER version 14: more
1045 genomes, a new PANTHER GO-slim and improvements in enrichment analysis tools, *Nucleic*
1046 *Acids Res.* **47**, D419–D426 (2019).
1047 29. T. M. Teslovich, K. Musunuru, A. V. Smith, A. C. Edmondson, I. M. Stylianou, M. Koseki, J.
1048 P. Pirruccello, S. Ripatti, D. I. Chasman, C. J. Willer, C. T. Johansen, S. W. Fouchier, A. Isaacs,
1049 G. M. Peloso, M. Barbalic, S. L. Ricketts, J. C. Bis, Y. S. Aulchenko, G. Thorleifsson, M. F.
1050 Feitosa, J. Chambers, M. Orho-Melander, O. Melander, T. Johnson, X. Li, X. Guo, M. Li, Y. Shin
1051 Cho, M. Jin Go, Y. Jin Kim, J.-Y. Lee, T. Park, K. Kim, X. Sim, R. Twee-Hee Ong, D. C.
1052 Croteau-Chonka, L. A. Lange, J. D. Smith, K. Song, J. Hua Zhao, X. Yuan, J. Luan, C. Lamina,
1053 A. Ziegler, W. Zhang, R. Y. L. Zee, A. F. Wright, J. C. M. Witteman, J. F. Wilson, G. Willemsen,
1054 H.-E. Wichmann, J. B. Whitfield, D. M. Waterworth, N. J. Wareham, G. Waeber, P.
1055 Vollenweider, B. F. Voight, V. Vitart, A. G. Uitterlinden, M. Uda, J. Tuomilehto, J. R. Thompson,
1056 T. Tanaka, I. Surakka, H. M. Stringham, T. D. Spector, N. Soranzo, J. H. Smit, J. Sinisalo, K.
1057 Silander, E. J. G. Sijbrands, A. Scuteri, J. Scott, D. Schlessinger, S. Sanna, V. Salomaa, J.
1058 Saharinen, C. Sabatti, A. Ruokonen, I. Rudan, L. M. Rose, R. Roberts, M. Rieder, B. M. Psaty,
1059 P. P. Pramstaller, I. Pichler, M. Perola, B. W. J. H. Penninx, N. L. Pedersen, C. Pattaro, A. N.
1060 Parker, G. Pare, B. A. Oostra, C. J. O'Donnell, M. S. Nieminen, D. A. Nickerson, G. W.
1061 Montgomery, T. Meitinger, R. McPherson, M. I. McCarthy, W. McArdle, D. Masson, N. G.
1062 Martin, F. Marroni, M. Mangino, P. K. E. Magnusson, G. Lucas, R. Luben, R. J. F. Loos, M.-L.
1063 Lokki, G. Lettre, C. Langenberg, L. J. Launer, E. G. Lakatta, R. Laaksonen, K. O. Kyvik, F.
1064 Kronenberg, I. R. König, K.-T. Khaw, J. Kaprio, L. M. Kaplan, Å. Johansson, M.-R. Jarvelin, A.
1065 Cecile J. W. Janssens, E. Ingelsson, W. Igl, G. Kees Hovingh, J.-J. Hottenga, A. Hofman, A. A.
1066 Hicks, C. Hengstenberg, I. M. Heid, C. Hayward, A. S. Havulinna, N. D. Hastie, T. B. Harris, T.
1067 Haritunians, A. S. Hall, U. Gyllensten, C. Guiducci, L. C. Groop, E. Gonzalez, C. Gieger, N. B.
1068 Freimer, L. Ferrucci, J. Erdmann, P. Elliott, K. G. Ejebe, A. Döring, A. F. Dominiczak, S.
1069 Demissie, P. Deloukas, E. J. C. de Geus, U. de Faire, G. Crawford, F. S. Collins, Y. I. Chen, M.
1070 J. Caulfield, H. Campbell, N. P. Burtt, L. L. Bonnycastle, D. I. Boomsma, S. M. Boekholdt, R. N.

Bergman, I. Barroso, S. Bandinelli, C. M. Ballantyne, T. L. Assimes, T. Quertermous, D. Altshuler, M. Seielstad, T. Y. Wong, E.-S. Tai, A. B. Feranil, C. W. Kuzawa, L. S. Adair, H. A. Taylor Jr, I. B. Borecki, S. B. Gabriel, J. G. Wilson, H. Holm, U. Thorsteinsdottir, V. Gudnason, R. M. Krauss, K. L. Mohlke, J. M. Ordovas, P. B. Munroe, J. S. Kooner, A. R. Tall, R. A. Hegele, J. J. P. Kastelein, E. E. Schadt, J. I. Rotter, E. Boerwinkle, D. P. Strachan, V. Mooser, K. Stefansson, M. P. Reilly, N. J. Samani, H. Schunkert, L. A. Cupples, M. S. Sandhu, P. M. Ridker, D. J. Rader, C. M. van Duijn, L. Peltonen, G. R. Abecasis, M. Boehnke, S. Kathiresan, Biological, clinical and population relevance of 95 loci for blood lipids, *Nature* **466**, 707–713 (2010).

30. P. Natarajan, G. M. Peloso, S. M. Zekavat, M. Montasser, A. Ganna, M. Chaffin, A. V. Khera, W. Zhou, J. M. Bloom, J. M. Engreitz, J. Ernst, J. R. O'Connell, S. E. Ruotsalainen, M. Alver, A. Manichaikul, W. C. Johnson, J. A. Perry, T. Poterba, C. Seed, I. L. Surakka, T. Esko, S. Ripatti, V. Salomaa, A. Correa, R. S. Vasan, M. Kellis, B. M. Neale, E. S. Lander, G. Abecasis, B. Mitchell, S. S. Rich, J. G. Wilson, L. A. Cupples, J. I. Rotter, C. J. Willer, S. Kathiresan, NHLBI TOPMed Lipids Working Group, Deep-coverage whole genome sequences and blood lipids among 16,324 individuals, *Nat. Commun.* **9**, 3391 (2018).

31. D. J. Liu, G. M. Peloso, H. Yu, A. S. Butterworth, X. Wang, A. Mahajan, D. Saleheen, C. Emdin, D. Alam, A. C. Alves, P. Amouyel, E. Di Angelantonio, D. Arveiler, T. L. Assimes, P. L. Auer, U. Baber, C. M. Ballantyne, L. E. Bang, M. Benn, J. C. Bis, M. Boehnke, E. Boerwinkle, J. Bork-Jensen, E. P. Bottinger, I. Brandslund, M. Brown, F. Busonero, M. J. Caulfield, J. C. Chambers, D. I. Chasman, Y. E. Chen, Y.-D. I. Chen, R. Chowdhury, C. Christensen, A. Y. Chu, J. M. Connell, F. Cucca, L. A. Cupples, S. M. Damrauer, G. Davies, I. J. Deary, G. Dedoussis, J. C. Denny, A. Dominiczak, M.-P. Dubé, T. Ebeling, G. Eiriksdottir, T. Esko, A.-E. Farmaki, M. F. Feitosa, M. Ferrario, J. Ferrieres, I. Ford, M. Fornage, P. W. Franks, T. M. Frayling, R. Frikke-Schmidt, L. G. Fritsche, P. Frossard, V. Fuster, S. K. Ganesh, W. Gao, M. E. Garcia, C. Gieger, F. Giulianini, M. O. Goodarzi, H. Grallert, N. Grarup, L. Groop, M. L. Grove, V. Gudnason, T. Hansen, T. B. Harris, C. Hayward, J. N. Hirschhorn, O. L. Holmen, J. Huffman, Y. Huo, K. Hveem, S. Jabeen, A. U. Jackson, J. Jakobsdottir, M.-R. Jarvelin, G. B. Jensen, M. E. Jørgensen, J. W. Jukema, J. M. Justesen, P. R. Kamstrup, S. Kanoni, F. Karpe, F. Kee, A. V Khera, D. Klarin, H. A. Koistinen, J. S. Kooner, C. Kooperberg, K. Kuulasmaa, J. Kuusisto, M. Laakso, T. Lakka, C. Langenberg, A. Langsted, L. J. Launer, T. Lauritzen, D. C. M. Liewald, L. A. Lin, A. Linneberg, R. J. F. Loos, Y. Lu, X. Lu, R. Mägi, A. Malarstig, A. Manichaikul, A. K. Manning, P. Mäntyselkä, E. Marouli, N. G. D. Masca, A. Maschio, J. B. Meigs, O. Melander, A. Metspalu, A. P. Morris, A. C. Morrison, A. Mulas, M. Müller-Nurasyid, P. B. Munroe, M. J. Neville, J. B. Nielsen, S. F. Nielsen, B. G. Nordestgaard, J. M. Ordovas, R. Mehran, C. J. O'Donnell, M. Orho-Melander, C. M. Molony, P. Muntendam, S. Padmanabhan, C. N. A. Palmer, D. Pasko, A. P. Patel, O. Pedersen, M. Perola, A. Peters, C. Pisinger, G. Pistis, O. Polasek, N. Poulter, B. M. Psaty, D. J. Rader, A. Rasheed, R. Rauramaa, D. F. Reilly, A. P. Reiner, F. Renström, S. S. Rich, P. M. Ridker, J. D. Rioux, N. R. Robertson, D. M. Roden, J. I. Rotter, I. Rudan, V. Salomaa, N. J. Samani, S. Sanna, N. Sattar, E. M. Schmidt, R. A. Scott, P. Sever, R. S. Sevilla, C. M. Shaffer, X. Sim, S. Sivapalaratnam, K. S. Small, A. V Smith, B. H. Smith, S. Somayajula, L. Southam, T. D. Spector, E. K. Speliotes, J. M. Starr, K. E. Stirrups, N. Stitziel, K. Strauch, H. M. Stringham, P. Surendran, H. Tada, A. R. Tall, H. Tang, J.-C. Tardif, K. D. Taylor, S. Trompet, P. S. Tsao, J. Tuomilehto, A. Tybjaerg-Hansen, N. R. van Zuydam, A. Varbo, T. V Varga, J. Virtamo, M. Waldenberger, N. Wang, N. J. Wareham, H. R. Warren, P. E. Weeke, J. Weinstock, J. Wessel, J. G. Wilson, P. W. F. Wilson, M. Xu, H. Yaghootkar, R. Young, E. Zeggini, H. Zhang, N. S. Zheng, W. Zhang, Y. Zhang, W. Zhou, Y. Zhou, M. Zoledziewska, J. M. M. Howson, J. Danesh, M. I. McCarthy, C. A. Cowan, G. Abecasis, P. Deloukas, K. Musunuru, C. J. Willer, S. Kathiresan, G. Abecasis, P. Deloukas, K. Musunuru, C. J. Willer, S. Kathiresan, Exome-wide association study of plasma lipids in >300,000 individuals, *Nat. Genet.* **49**, 1758–1766 (2017).

1122 32. C. Bycroft, C. Freeman, D. Petkova, G. Band, L. T. Elliott, K. Sharp, A. Motyer, D. Vukcevic,
1123 O. Delaneau, J. O'Connell, A. Cortes, S. Welsh, A. Young, M. Effingham, G. McVean, S. Leslie,
1124 N. Allen, P. Donnelly, J. Marchini, The UK Biobank resource with deep phenotyping and
1125 genomic data, *Nature* (2018), doi:10.1038/s41586-018-0579-z.
1126 33. A. Loregger, J. K. Nelson, N. Zelcer, in *Methods in molecular biology (Clifton, N.J.)*, (2017),
1127 vol. 1583, pp. 53–63.
1128 34. A. Mazein, S. Watterson, W. Y. Hsieh, W. J. Griffiths, P. Ghazal, A comprehensive machine-
1129 readable view of the mammalian cholesterol biosynthesis pathway, *Biochem. Pharmacol.*
1130 (2013), doi:10.1016/j.bcp.2013.03.021.
1131 35. R. B. Rose, J. H. Bayle, J. A. Endrizzi, J. D. Cronk, G. R. Crabtree, T. Alber, Structural basis
1132 of dimerization, coactivator recognition and MODY3 mutations in HNF-1α, *Nat. Struct. Biol.*
1133 (2000), doi:10.1038/78966.
1134 36. A. Delaforest, F. Di Furio, R. Jing, A. Ludwig-Kubinski, K. Twaroski, A. Urick, K. Pulakanti,
1135 S. Rao, S. A. Duncan, HNF4A regulates the formation of hepatic progenitor cells from human
1136 iPSC-derived endoderm by facilitating efficient recruitment of RNA pol II, *Genes (Basel).* (2019),
1137 doi:10.3390/genes10010021.
1138 37. K. Wang, A. X. Holterman, Pathophysiologic role of hepatocyte nuclear factor 6*Cell. Signal.*
1139 (2012), doi:10.1016/j.cellsig.2011.08.009.
1140 38. U. Wellner, J. Schubert, U. C. Burk, O. Schmalhofer, F. Zhu, A. Sonntag, B. Waldvogel, C.
1141 Vannier, D. Darling, A. Zur Hausen, V. G. Brunton, J. Morton, O. Sansom, J. Schüler, M. P.
1142 Stemmler, C. Herzberger, U. Hopt, T. Keck, S. Brabletz, T. Brabletz, The EMT-activator ZEB1
1143 promotes tumorigenicity by repressing stemness-inhibiting microRNAs, *Nat. Cell Biol.* (2009),
1144 doi:10.1038/ncb1998.
1145 39. C. L. Gao, J. G. Zhu, Y. P. Zhao, X. H. Chen, C. B. Ji, C. M. Zhang, C. Zhu, Z. K. Xia, Y. Z.
1146 Peng, X. R. Guo, Mitochondrial dysfunction is induced by the overexpression of UCP4 in 3T3-L1
1147 adipocytes, *Int. J. Mol. Med.* (2010), doi:10.3892/ijmm_00000315.
1148 40. F. Quazi, R. S. Molday, Differential phospholipid substrates and directional transport by
1149 ATP-binding cassette proteins ABCA1, ABCA7, and ABCA4 and disease-causing mutants, *J.*
1150 *Biol. Chem.* (2013), doi:10.1074/jbc.M113.508812.
1151 41. J. E. Kung, N. Jura, The pseudokinase TRIB 1 toggles an intramolecular switch to regulate
1152 COP 1 nuclear export , *EMBO J.* (2019), doi:10.15252/embj.201899708.
1153 42. J. M. Murphy, Y. Nakatani, S. A. Jamieson, W. Dai, I. S. Lucet, P. D. Mace, Molecular
1154 Mechanism of CCAAT-Enhancer Binding Protein Recruitment by the TRIB1 Pseudokinase,
1155 *Structure* (2015), doi:10.1016/j.str.2015.08.017.
1156 43. S. Soubeyrand, A. Martinuk, R. McPherson, TRIB1 is a positive regulator of hepatocyte
1157 nuclear factor 4-Alpha, *Sci. Rep.* (2017), doi:10.1038/s41598-017-05768-1.
1158 44. R. C. Bauer, M. Sasaki, D. M. Cohen, J. Cui, M. A. Smith, B. O. Yenilmez, D. J. Steger, D. J.
1159 Rader, Tribbles-1 regulates hepatic lipogenesis through posttranscriptional regulation of
1160 C/EBPα, *J. Clin. Invest.* (2015), doi:10.1172/JCI77095.
1161 45. R. Burkhardt, S. A. Toh, W. R. Lagor, A. Birkeland, M. Levin, X. Li, M. Robblee, V. D.
1162 Fedorov, M. Yamamoto, T. Satoh, S. Akira, S. Kathiresan, J. L. Breslow, D. J. Rader, Trib1 is a
1163 lipid- and myocardial infarction-associated gene that regulates hepatic lipogenesis and VLDL
1164 production in mice, *J. Clin. Invest.* **120**, 4410–4414 (2010).
1165 46. A. Motley, N. A. Bright, M. N. J. Seaman, M. S. Robinson, Clathrin-mediated endocytosis in
1166 AP-2-depleted cells, *J. Cell Biol.* (2003), doi:10.1083/jcb.200305145.
1167 47. S. F. Parsons, G. Mallinson, C. H. Holmes, J. M. Houlihan, K. L. Simpson, W. J. Mawby, N.
1168 K. Spurr, D. Warne, A. N. Barclay, D. J. Anstee, The Lutheran blood group glycoprotein, another
1169 member of the immunoglobulin superfamily, is widely expressed in human tissues and is
1170 developmentally regulated in human liver, *Proc. Natl. Acad. Sci. U. S. A.* (1995),
1171 doi:10.1073/pnas.92.12.5496.
1172 48. S. K. Mishra, P. A. Keyel, M. A. Edeling, A. L. Dupin, D. J. Owen, L. M. Traub, Functional

1173 dissection of an AP-2 β2 appendage-binding sequence within the autosomal recessive
1174 hypercholesterolemia protein, *J. Biol. Chem.* (2005), doi:10.1074/jbc.M501029200.
1175 49. A. Radhakrishnan, J. L. Goldstein, J. G. McDonald, M. S. Brown, Switch-like Control of
1176 SREBP-2 Transport Triggered by Small Changes in ER Cholesterol: A Delicate Balance, *Cell*
1177 *Metab.* (2008), doi:10.1016/j.cmet.2008.10.008.
1178 50. J. D. Horton, N. A. Shah, J. A. Warrington, N. N. Anderson, S. W. Park, M. S. Brown, J. L.
1179 Goldstein, Combined analysis of oligonucleotide microarray data from transgenic and knockout
1180 mice identifies direct SREBP target genes., *Proc. Natl. Acad. Sci. U. S. A.* **100**, 12027–32
1181 (2003).
1182 51. Scandinavian Simvastatin Survival Study Group, Randomised trial of cholesterol lowering in
1183 4444 patients with coronary heart disease: the Scandinavian Simvastatin Survival Study (4S),
1184 *Lancet* (1994), doi:10.1016/S0140-6736(94)90566-5.
1185 52. N. G. Lintner, K. F. McClure, D. Petersen, A. T. Londregan, D. W. Piotrowski, L. Wei, J.
1186 Xiao, M. Bolt, P. M. Loria, B. Maguire, K. F. Geoghegan, A. Huang, T. Rolph, S. Liras, J. A.
1187 Doudna, R. G. Dullea, J. H. D. Cate, C. Khosla, Ed. Selective stalling of human translation
1188 through small-molecule engagement of the ribosome nascent chain., *PLoS Biol.* **15**, e2001882
1189 (2017).
1190 53. W. Li, F. R. Ward, K. F. McClure, S. T.-L. Chang, E. Montabana, S. Liras, R. G. Dullea, J. H.
1191 D. Cate, Structural basis for selective stalling of human ribosome nascent chain complexes by a
1192 drug-like molecule, *Nat. Struct. Mol. Biol.* **26**, 501–509 (2019).
1193 54. T. Suzuki, M. Terasaki, C. Takemoto-Hori, T. Hanada, T. Ueda, A. Wada, K. Watanabe,
1194 Structural compensation for the deficit of rRNA with proteins in the mammalian mitochondrial
1195 ribosome. Systematic analysis of protein components of the large ribosomal subunit from
1196 mammalian mitochondria, *J. Biol. Chem.* (2001), doi:10.1074/jbc.M100432200.
1197 55. P. J. Thul, L. Akesson, M. Wiking, D. Mahdessian, A. Geladaki, H. Ait Blal, T. Alm, A.
1198 Asplund, L. Björk, L. M. Breckels, A. Bäckström, F. Danielsson, L. Fagerberg, J. Fall, L. Gatto,
1199 C. Gnann, S. Hober, M. Hjelmare, F. Johansson, S. Lee, C. Lindskog, J. Mulder, C. M. Mulvey,
1200 P. Nilsson, P. Oksvold, J. Rockberg, R. Schutten, J. M. Schwenk, A. Sivertsson, E. Sjöstedt, M.
1201 Skogs, C. Stadler, D. P. Sullivan, H. Tegel, C. Winsnes, C. Zhang, M. Zwahlen, A. Mardinoglu,
1202 F. Pontén, K. Von Feilitzen, K. S. Lilley, M. Uhlén, E. Lundberg, A subcellular map of the human
1203 proteome, *Science (80-.).* (2017), doi:10.1126/science.aal3321.
1204 56. H. Li, B. Dong, S. W. Park, H.-S. Lee, W. Chen, J. Liu, Hepatocyte nuclear factor 1alpha
1205 plays a critical role in PCSK9 gene transcription and regulation by the natural
1206 hypocholesterolemic compound berberine., *J. Biol. Chem.* **284**, 28885–95 (2009).
1207 57. A.-X. Guo, J.-J. Cui, L.-Y. Wang, J.-Y. Yin, The role of CSDE1 in translational
1208 reprogramming and human diseases, *Cell Commun. Signal.* **18**, 14 (2020).
1209 58. M. Dinur, R. Kilav, A. Sela-Brown, H. Jacquemin-Sablon, T. Naveh-Many, In vitro evidence
1210 that upstream of N-ras participates in the regulation of parathyroid hormone messenger
1211 ribonucleic acid stability, *Mol. Endocrinol.* (2006), doi:10.1210/me.2005-0333.
1212 59. K. S. Moore, N. Yagci, F. Van Alphen, N. A. Paolini, R. Horos, N. M. Held, R. H.
1213 Houtkooper, E. Van Den Akker, A. B. Meijer, P. A. C. T'Hoen, M. Von Lindern, Csde1 binds
1214 transcripts involved in protein homeostasis and controls their expression in an erythroid cell line,
1215 *Sci. Rep.* (2018), doi:10.1038/s41598-018-20518-7.
1216 60. T. C. Chang, A. Yamashita, C. Y. A. Chen, Y. Yamashita, W. Zhu, S. Durdan, A. Kahvejian,
1217 N. Sonenberg, A. Bin Shyu, UNR, a new partner of poly(A)-binding protein, plays a key role in
1218 translationally coupled mRNA turnover mediated by the c-fos major coding-region determinant,
1219 *Genes Dev.* (2004), doi:10.1101/gad.1219104.
1220 61. G. M. Wilson, M. Z. Vasa, R. G. Deeley, Stabilization and cytoskeletal-association of LDL
1221 receptor mRNA are mediated by distinct domains in its 3' untranslated region, *J. Lipid Res.*
1222 (1998).
1223 62. H. Li, W. Chen, Y. Zhou, P. Abidi, O. Sharpe, W. H. Robinson, F. B. Kraemer, J. Liu,

1224 Identification of mRNA binding proteins that regulate the stability of LDL receptor mRNA through
1225 AU-rich elements, *J. Lipid Res.* (2009), doi:10.1194/jlr.M800375-JLR200.
1226 63. K. Bjune, L. Wierød, S. Naderi, Triciribine increases LDLR expression and LDL uptake
1227 through stabilization of LDLR mRNA, *Sci. Rep.* (2018), doi:10.1038/s41598-018-34237-6.
1228 64. T. Bakheet, M. Frevel, B. R. G. Williams, W. Greer, K. S. A. Khabar, ARED: Human AU-rich
1229 element-containing mRNA database reveals an unexpectedly diverse functional repertoire of
1230 encoded proteins, *Nucleic Acids Res.* (2001), doi:10.1093/nar/29.1.246.
1231 65. R. S. Wu, I. I. Lam, H. Clay, D. N. Duong, R. C. Deo, S. R. Coughlin, A Rapid Method for
1232 Directed Gene Knockout for Screening in G0 Zebrafish., *Dev. Cell* **46**, 112-125.e4 (2018).
1233 66. C. Liu, Y. S. Kim, J. Kim, J. Pattison, A. Kamaid, Y. I. Miller, Modeling hypercholesterolemia
1234 and vascular lipid accumulation in LDL receptor mutant zebrafish, *J. Lipid Res.* **59**, 391–399
1235 (2018).
1236 67. A. B. Singh, H. Li, C. F. K. Kan, B. Dong, M. R. Nicolls, J. Liu, The critical role of mRNA
1237 destabilizing protein heterogeneous nuclear ribonucleoprotein D in 3′ untranslated region-
1238 mediated decay of low-density lipoprotein receptor mRNA in liver tissue, *Arterioscler. Thromb.*
1239 *Vasc. Biol.* (2014), doi:10.1161/ATVBAHA.112.301131.
1240 68. B. Paigen, A. Morrow, C. Brandon, D. Mitchell, P. Holmes, Variation in susceptibility to
1241 atherosclerosis among inbred strains of mice, *Atherosclerosis* (1985), doi:10.1016/0021-
1242 9150(85)90138-8.
1243 69. G. S. Getz, C. A. Reardon, Diet and murine atherosclerosis*Arterioscler. Thromb. Vasc. Biol.*
1244 (2006), doi:10.1161/01.ATV.0000201071.49029.17.
1245 70. M. von Scheidt, Y. Zhao, Z. Kurt, C. Pan, L. Zeng, X. Yang, H. Schunkert, A. J. Lusis,
1246 Applications and Limitations of Mouse Models for Understanding Human Atherosclerosis*Cell*
1247 *Metab.* (2017), doi:10.1016/j.cmet.2016.11.001.
1248 71. R. Collins, C. Reith, J. Emberson, J. Armitage, C. Baigent, L. Blackwell, R. Blumenthal, J.
1249 Danesh, G. D. Smith, D. DeMets, S. Evans, M. Law, S. MacMahon, S. Martin, B. Neal, N.
1250 Poulter, D. Preiss, P. Ridker, I. Roberts, A. Rodgers, P. Sandercock, K. Schulz, P. Sever, J.
1251 Simes, L. Smeeth, N. Wald, S. Yusuf, R. Peto, Interpretation of the evidence for the efficacy and
1252 safety of statin therapy, *Lancet* **388**, 2532–2561 (2016).
1253 72. B. T. Emmer, E. J. Sherman, P. J. Lascuna, S. E. Graham, C. J. Willer, D. Ginsburg,
1254 Genome-scale CRISPR screening for modifiers of cellular LDL uptake, *PLOS Genet.* (2021),
1255 doi:10.1371/journal.pgen.1009285.
1256 73. M. N. Trinh, M. S. Brown, J. L. Goldstein, J. Han, G. Vale, J. G. McDonald, J. Seemann, J.
1257 T. Mendell, F. Lu, Last step in the path of LDL cholesterol from lysosome to plasma membrane
1258 to ER is governed by phosphatidylserine, *Proc. Natl. Acad. Sci. U. S. A.* (2020),
1259 doi:10.1073/pnas.2010682117.
1260 74. C. Knouff, S. Malloy, J. Wilder, M. K. Altenburg, N. Maeda, Doubling Expression of the Low
1261 Density Lipoprotein Receptor by Truncation of the 3′-Untranslated Region Sequence
1262 Ameliorates Type III Hyperlipoproteinemia in Mice Expressing the Human ApoE2 Isoform, *J.*
1263 *Biol. Chem.* (2001), doi:10.1074/jbc.M009423200.
1264 75. W. Kong, J. Wei, P. Abidi, M. Lin, S. Inaba, C. Li, Y. Wang, Z. Wang, S. Si, H. Pan, S.
1265 Wang, J. Wu, Y. Wang, Z. Li, J. Liu, J. D. Jiang, Berberine is a novel cholesterol-lowering drug
1266 working through a unique mechanism distinct from statins, *Nat. Med.* (2004),
1267 doi:10.1038/nm1135.
1268 76. H. Ju Lee, D. Bartsch, C. Xiao, S. Guerrero, G. Ahuja, C. Schindler, J. J. Moresco, J. R.
1269 Yates, F. Gebauer, H. Bazzi, C. Dieterich, L. Kurian, D. Vilchez, A post-transcriptional program
1270 coordinated by CSDE1 prevents intrinsic neural differentiation of human embryonic stem cells,
1271 *Nat. Commun.* (2017), doi:10.1038/s41467-017-01744-5.
1272 77. O. Boussadia, M. Niepmann, L. Créancier, A.-C. Prats, F. Dautry, H. Jacquemin-Sablon,
1273 Unr Is Required In Vivo for Efficient Initiation of Translation from the Internal Ribosome Entry
1274 Sites of both Rhinovirus and Poliovirus, *J. Virol.* (2003), doi:10.1128/jvi.77.6.3353-3359.2003.

1275 78. V. Dormoy-Raclet, J. Markovits, A. Jacquemin-Sablon, H. Jacquemin-Sablon, Regulation of
1276 Unr expression by 5′- and 3′-untranslated regions of its mRNA through modulation of stability
1277 and IRES mediated translation, *RNA Biol.* (2005), doi:10.4161/rna.2.3.2203.
1278 79. K. E. Duncan, C. Strein, M. W. Hentze, The SXL-UNR Corepressor Complex Uses a PABP-
1279 Mediated Mechanism to Inhibit Ribosome Recruitment to msl-2 mRNA, *Mol. Cell* (2009),
1280 doi:10.1016/j.molcel.2009.09.042.
1281 80. S. Ray, E. C. Anderson, Stimulation of translation by human Unr requires cold shock
1282 domains 2 and 4, and correlates with poly(A) binding protein interaction, *Sci. Rep.* (2016),
1283 doi:10.1038/srep22461.
1284 81. H. Guo, Y. Li, L. Shen, T. Wang, X. Jia, L. Liu, T. Xu, M. Ou, K. Hoekzema, H. Wu, M. A.
1285 Gillentine, C. Liu, H. Ni, P. Peng, R. Zhao, Y. Zhang, C. Phornphutkul, A. P. A. Stegmann, C. E.
1286 Prada, R. J. Hopkin, J. T. Shieh, K. McWalter, K. G. Monaghan, P. M. van Hasselt, K. van
1287 Gassen, T. Bai, M. Long, L. Han, Y. Quan, M. Chen, Y. Zhang, K. Li, Q. Zhang, J. Tan, T. Zhu,
1288 Y. Liu, N. Pang, J. Peng, D. A. Scott, S. R. Lalani, M. Azamian, G. M. S. Mancini, D. J. Adams,
1289 M. Kvarnung, A. Lindstrand, A. Nordgren, J. Pevsner, I. A. Osei-Owusu, C. Romano, G.
1290 Calabrese, O. Galesi, J. Gecz, E. Haan, J. Ranells, M. Racobaldo, M. Nordenskjold, S. Madan-
1291 Khetarpal, J. Sebastian, S. Ball, X. Zou, J. Zhao, Z. Hu, F. Xia, P. Liu, J. A. Rosenfeld, B. B. A.
1292 de Vries, R. A. Bernier, Z. Q. D. Xu, H. Li, W. Xie, R. B. Hufnagel, E. E. Eichler, K. Xia,
1293 Disruptive variants of CSDE1 associate with autism and interfere with neuronal development
1294 and synaptic transmission, *Sci. Adv.* (2019), doi:10.1126/sciadv.aax2166.
1295 82. L. Wurth, P. Papasaikas, D. Olmeda, N. Bley, G. T. Calvo, S. Guerrero, D. Cerezo-Wallis, J.
1296 Martinez-Useros, M. García-Fernández, S. Hüttelmaier, M. S. Soengas, F. Gebauer,
1297 UNR/CSDE1 Drives a Post-transcriptional Program to Promote Melanoma Invasion and
1298 Metastasis, *Cancer Cell* (2016), doi:10.1016/j.ccell.2016.10.004.
1299 83. P. Gennemark, K. Walter, N. Clemmensen, D. Rekić, C. A. M. Nilsson, J. Knöchel, M.
1300 Hölttä, L. Wernevik, B. Rosengren, D. Kakol-Palm, Y. Wang, R. Z. Yu, R. S. Geary, S. J. Riney,
1301 B. P. Monia, R. Isaksson, R. Jansson-Löfmark, C. S. J. Rocha, D. Lindén, E. Hurt-Camejo, R.
1302 Crooke, L. Tillman, T. Rydén-Bergsten, B. Carlsson, U. Andersson, M. Elebring, A. Tivesten, N.
1303 Davies, An oral antisense oligonucleotide for PCSK9 inhibition, *Sci. Transl. Med.* **13**, eabe9117
1304 (2021).
1305 84. K. Musunuru, A. C. Chadwick, T. Mizoguchi, S. P. Garcia, J. E. DeNizio, C. W. Reiss, K.
1306 Wang, S. Iyer, C. Dutta, V. Clendaniel, M. Amaonye, A. Beach, K. Berth, S. Biswas, M. C.
1307 Braun, H.-M. Chen, T. V Colace, J. D. Ganey, S. A. Gangopadhyay, R. Garrity, L. N. Kasiewicz,
1308 J. Lavoie, J. A. Madsen, Y. Matsumoto, A. M. Mazzola, Y. S. Nasrullah, J. Nneji, H. Ren, A.
1309 Sanjeev, M. Shay, M. R. Stahley, S. H. Y. Fan, Y. K. Tam, N. M. Gaudelli, G. Ciaramella, L. E.
1310 Stolz, P. Malyala, C. J. Cheng, K. G. Rajeev, E. Rohde, A. M. Bellinger, S. Kathiresan, In vivo
1311 CRISPR base editing of PCSK9 durably lowers cholesterol in primates, *Nature* **593**, 429–434
1312 (2021).
1313 85. K. F. McClure, D. W. Piotrowski, D. Petersen, L. Wei, J. Xiao, A. T. Londregan, A. S.
1314 Kamlet, A.-M. Dechert-Schmitt, B. Raymer, R. B. Ruggeri, D. Canterbury, C. Limberakis, S.
1315 Liras, P. DaSilva-Jardine, R. G. Dullea, P. M. Loria, B. Reidich, C. T. Salatto, H. Eng, E. Kimoto,
1316 K. Atkinson, A. King-Ahmad, D. Scott, K. Beaumont, J. R. Chabot, M. W. Bolt, K. Maresca, K.
1317 Dahl, R. Arakawa, A. Takano, C. Halldin, Liver-Targeted Small-Molecule Inhibitors of Proprotein
1318 Convertase Subtilisin/Kexin Type 9 Synthesis, *Angew. Chemie Int. Ed.* **56**, 16218–16222
1319 (2017).
1320 86. J. Martinez-Useros, N. Garcia-Carbonero, W. Li, M. J. Fernandez-Aceñero, I. Cristobal, R.
1321 Rincon, M. Rodriguez-Remirez, A. Borrero-Palacios, J. Garcia-Foncillas, UNR/CSDE1
1322 Expression Is Critical to Maintain Invasive Phenotype of Colorectal Cancer through Regulation
1323 of c-MYC and Epithelial-to-Mesenchymal Transition, *J. Clin. Med.* (2019),
1324 doi:10.3390/jcm8040560.
1325 87. V. Dormoy-Raclet, J. Markovits, Y. Malato, S. Huet, P. Lagarde, D. Montaudon, A.

1326 Jacquemin-Sablon, H. Jacquemin-Sablon, Unr, a cytoplasmic RNA-binding protein with cold-
1327 shock domains, is involved in control of apoptosis in ES and HuH7 cells, *Oncogene* (2007),
1328 doi:10.1038/sj.onc.1210068.
1329 88. N. Matsuzawa, T. Takamura, S. Kurita, H. Misu, T. Ota, H. Ando, M. Yokoyama, M. Honda,
1330 Y. Zen, Y. Nakanuma, K. I. Miyamoto, S. Kaneko, Lipid-induced oxidative stress causes
1331 steatohepatitis in mice fed an atherogenic diet, *Hepatology* (2007), doi:10.1002/hep.21874.
1332 89. J. J. V McMurray, M. Packer, A. S. Desai, J. Gong, M. P. Lefkowitz, A. R. Rizkala, J. L.
1333 Rouleau, V. C. Shi, S. D. Solomon, K. Swedberg, M. R. Zile, Angiotensin–Neprilysin Inhibition
1334 versus Enalapril in Heart Failure, *N. Engl. J. Med.* **371**, 993–1004 (2014).
1335 90. D. G. Gibson, L. Young, R.-Y. Chuang, J. C. Venter, C. A. Hutchison, H. O. Smith,
1336 Enzymatic assembly of DNA molecules up to several hundred kilobases., *Nat. Methods* **6**, 343–
1337 5 (2009).
1338 91. J. S. Chorba, A. M. Galvan, K. M. Shokat, Stepwise processing analyses of the single-
1339 turnover PCSK9 protease reveal its substrate sequence specificity and link clinical genotype to
1340 lipid phenotype, *J. Biol. Chem.* **293**, 1875–1886 (2018).
1341 92. J. H. Kim, S.-R. Lee, L.-H. Li, H.-J. Park, J.-H. Park, K. Y. Lee, M.-K. Kim, B. A. Shin, S.-Y.
1342 Choi, V. Thiel, Ed. High Cleavage Efficiency of a 2A Peptide Derived from Porcine Teschovirus-
1343 1 in Human Cell Lines, Zebrafish and Mice, *PLoS One* **6**, e18556 (2011).
1344 93. D. G. Gibson, H. O. Smith, C. A. Hutchison, J. C. Venter, C. Merryman, Chemical synthesis
1345 of the mouse mitochondrial genome, *Nat. Methods* (2010), doi:10.1038/nmeth.1515.
1346 94. H. Mi, A. Muruganujan, X. Huang, D. Ebert, C. Mills, X. Guo, P. D. Thomas, Protocol Update
1347 for large-scale genome and gene function analysis with the PANTHER classification system
1348 (v.14.0), *Nat. Protoc.* (2019), doi:10.1038/s41596-019-0128-8.
1349 95. A. Bateman, UniProt: A worldwide hub of protein knowledge, *Nucleic Acids Res.* (2019),
1350 doi:10.1093/nar/gky1049.
1351 96. C. Sudlow, J. Gallacher, N. Allen, V. Beral, P. Burton, J. Danesh, P. Downey, P. Elliott, J.
1352 Green, M. Landray, B. Liu, P. Matthews, G. Ong, J. Pell, A. Silman, A. Young, T. Sprosen, T.
1353 Peakman, R. Collins, UK Biobank: An Open Access Resource for Identifying the Causes of a
1354 Wide Range of Complex Diseases of Middle and Old Age, *PLoS Med.* (2015),
1355 doi:10.1371/journal.pmed.1001779.
1356 97. P. R. Loh, G. Tucker, B. K. Bulik-Sullivan, B. J. Vilhjálmsson, H. K. Finucane, R. M. Salem,
1357 D. I. Chasman, P. M. Ridker, B. M. Neale, B. Berger, N. Patterson, A. L. Price, Efficient
1358 Bayesian mixed-model analysis increases association power in large cohorts, *Nat. Genet.*
1359 (2015), doi:10.1038/ng.3190.
1360 98. J. M. Baker, F. M. Boyce, High-throughput functional screening using a homemade dual-
1361 glow luciferase assay, *J. Vis. Exp.* (2014), doi:10.3791/50282.
1362 99. M. I. Love, W. Huber, S. Anders, Moderated estimation of fold change and dispersion for
1363 RNA-seq data with DESeq2, *Genome Biol.* (2014), doi:10.1186/s13059-014-0550-8.
1364 100. M. D. Robinson, D. J. McCarthy, G. K. Smyth, edgeR: a Bioconductor package for
1365 differential expression analysis of digital gene expression data., *Bioinformatics* **26**, 139–140
1366 (2010).
1367 101. A. T. L. Lun, Y. Chen, G. K. Smyth, It's DE-licious: A Recipe for Differential Expression
1368 Analyses of RNA-seq Experiments Using Quasi-Likelihood Methods in edgeR., *Methods Mol.*
1369 *Biol.* **1418**, 391–416 (2016).
1370 102. M. V. Kuleshov, M. R. Jones, A. D. Rouillard, N. F. Fernandez, Q. Duan, Z. Wang, S.
1371 Koplev, S. L. Jenkins, K. M. Jagodnik, A. Lachmann, M. G. McDermott, C. D. Monteiro, G. W.
1372 Gundersen, A. Ma'ayan, Enrichr: a comprehensive gene set enrichment analysis web server
1373 2016 update, *Nucleic Acids Res.* (2016), doi:10.1093/nar/gkw377.
1374 103. Z. Gu, R. Eils, M. Schlesner, Complex heatmaps reveal patterns and correlations in
1375 multidimensional genomic data., *Bioinformatics* **32**, 2847–2849 (2016).
1376 104. G. S. (editors). Higgins JPT, Cochrane Handbook for Systematic Reviews of Interventions

Version 5.1.0 *Cochrane Collab.* (2011).
105. M. Roederer, W. Moore, A. Treister, R. R. Hardy, L. A. Herzenberg, Probability binning comparison: A metric for quantitating multivariate distribution differences, *Cytometry* (2001), doi:10.1002/1097-0320(20010901)45:1<47::AID-CYTO1143>3.0.CO;2-A.
106. M. Roederer, A. Treister, W. Moore, L. A. Herzenberg, Probability binning comparison: A metric for quantitating univariate distribution differences, *Cytometry* (2001), doi:10.1002/1097-0320(20010901)45:1<37::AID-CYTO1142>3.0.CO;2-E.
107. M. Roederer, R. R. Hardy, Frequency difference gating: A multivariate method for identifying subsets that differ between samples, *Cytometry* (2001), doi:10.1002/1097-0320(20010901)45:1<56::AID-CYTO1144>3.0.CO;2-9.

Figures and Figure Legends

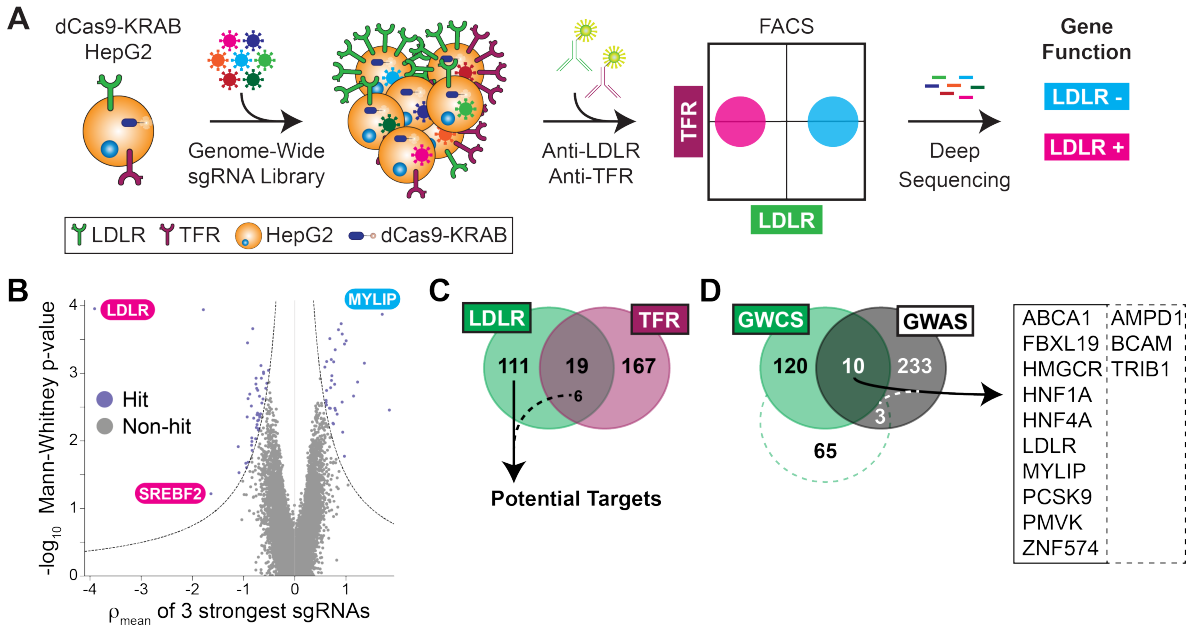

Figure 1: Genome-Wide CRISPR Interference Screen. *A)* Overall schematic of selection. See text for details. *B)* Volcano plot showing the statistical significance (Mann-Whitney test) of the guides recovered for each gene against the mean ρ phenotype of the three guides with the strongest effect. ρ is defined as the $\log_2$-fold enrichment for high LDLR expressing cells to the low LDLR expressing cells. Guides targeting known regulators of the LDLR are noted. *C)* Venn diagram showing the overlap between parallel LDLR and TFR screens. 6 guides common to both had opposing expression phenotypes in the respective screens and were included as specific hits. *D)* Venn diagram of hits between the LDLR screen (GWCS) and putative genes correlated with serum LDL from GWAS. The dotted line indicates a relaxed threshold for hit selection from LDLR screen, with only an additional 3 genes in the overlap. Overlap genes shown at right.

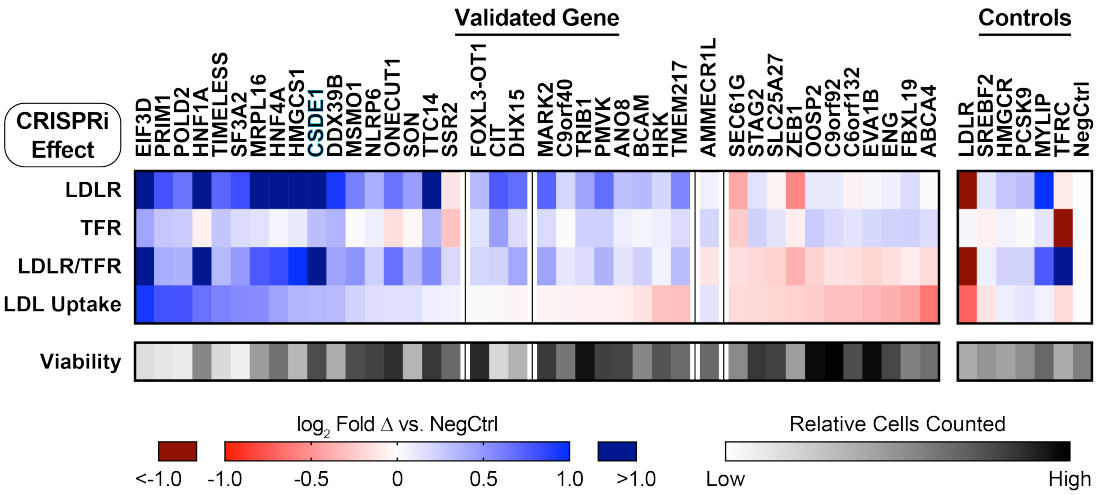

Figure 2: Validation of LDLR CRISPRi Hits. Heatmap showing receptor abundance (LDLR, TFR, and LDLR/TFR ratio) and function (LDL uptake) for dCas9-KRAB HepG2 cells transduced with sgRNA targeting the indicated gene, analyzed by flow cytometry. Hits are grouped according to directional effect on LDLR abundance, and then within groups, by effect on LDL uptake (with uptake from *FOXL3-OT1*, *CIT*, and *DHX15* sgRNAs not significantly different from negative control sgRNA). *CSDE1* highlighted in blue. Control sgRNAs shown at right. Readouts show $\log_2$ fold change compared to transduction with negative control sgRNA and represent the weighted average of the effects from both sgRNAs targeting each gene. Viability indicates the relative number of cells surviving to flow cytometry in the experiments. Functional classification of genes is shown visually in Supp. Fig. 3. Note that LDLR/TFR is a separately ascertained value from individual cells, and not a derived parameter from aggregate data. Only the hits for which two separate sgRNAs independently validated for receptor expression are shown, defined as $p < 0.05$ via Holm-Sidak corrected T-test. Data represent summary information from 3 to 4 independent experiments.

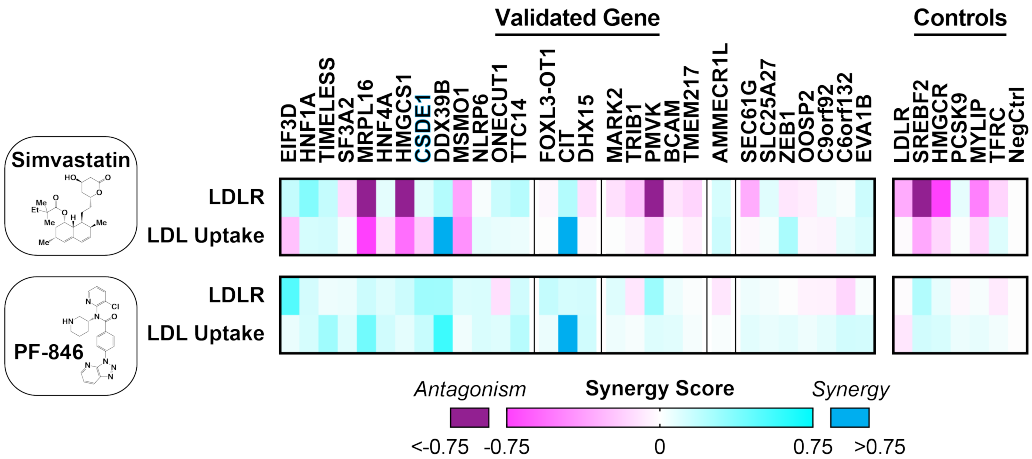

Figure 3: CRISPRi Knockdown Synergy with Statin and PF-846. Heatmap showing synergy score with statin (top) or PF-846 (bottom) for knockdowns of indicated validated genes with a single sgRNA for separate LDLR abundance and function experiments. Hits are grouped first according to overall effect on LDLR abundance, and secondarily by effect on LDL uptake, as in Fig. 2. *CSDE1* highlighted in blue. Data represent summary information from 4 independent experiments.

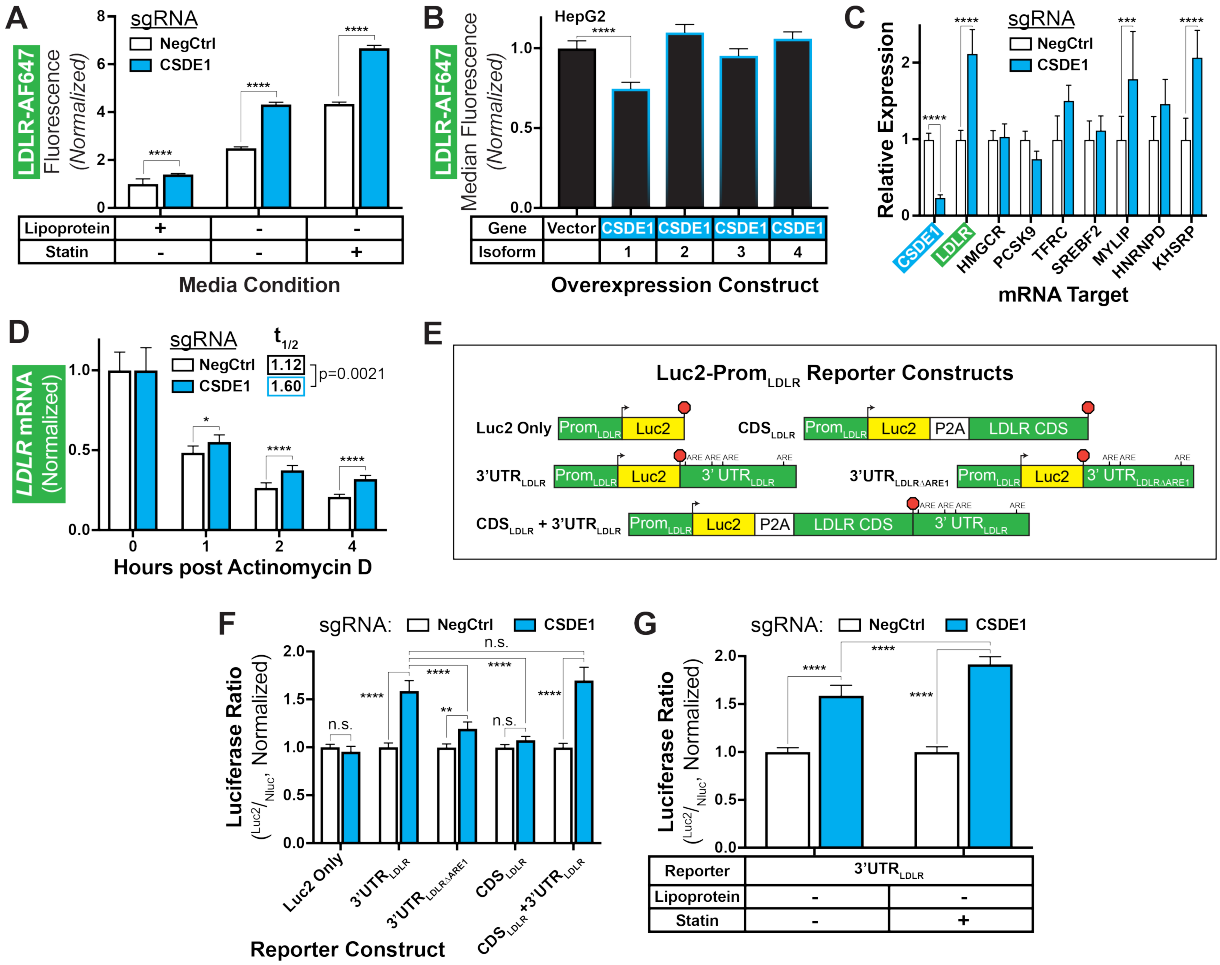

Figure 4: CSDE1 Mediates *LDLR* mRNA Decay. *A)* Relative LDLR abundance, by normalized mean fluorescence, in engineered dCas9-KRAB HepG2 cells transduced with indicated sgRNAs (CRISPRi cells) and grown in the indicated media conditions. *B)* Relative LDLR abundance, by normalized median fluorescence, in HepG2 cells overexpressing indicated CSDE1 isoforms. One-way ANOVA with Tukey's multiple comparisons test shown. *C)* Relative expression, by qPCR, of indicated mRNA targets in CRISPRi cells under sterol-depleted conditions. *D)* Relative expression, by qPCR, of *LDLR* mRNA in CRISPRi cells after arrest of transcription with actinomycin D. Data are normalized to results at T=0 within the sgRNA evaluated to illustrate the change in time. $t_{1/2}$ shown indicates the best fit data to a one-stage exponential decay equation. Unpaired t-tests with Holm-Sidak correction shown for pairwise comparisons. Extra sum-of-squares F test shown for decay equation. *E)* Schematics of Luc2-$Prom_{LDLR}$ reporter constructs, illustrating *LDLR* promoter, start site (arrowhead), P2A ribosomal skipping sequence (if present), AREs in 3' UTR, stop codon (red octagon), and indicated regions of the *LDLR* gene. ARE = Adenylate-uridylate (AU) rich element. Schematics not to scale. *F)* Ratiometric luciferase outputs, normalized to negative control, of CRISPRi cells transfected with indicated luciferase constructs. *G)* Ratiometric luciferase outputs of 3' UTR addended luciferase constructs in CRISPRi cells. *All panels)* Error bars indicate 95% confidence intervals. Data represent summary information from 3-4 independent experiments. n.s. = not significant, * = $p < 0.05$, ** = $p < 0.01$, *** = $p < 0.001$, and **** = $p < 0.0001$. Unless otherwise indicated, two-way ANOVA with Sidak's multiple comparisons test was used for statistical analysis.

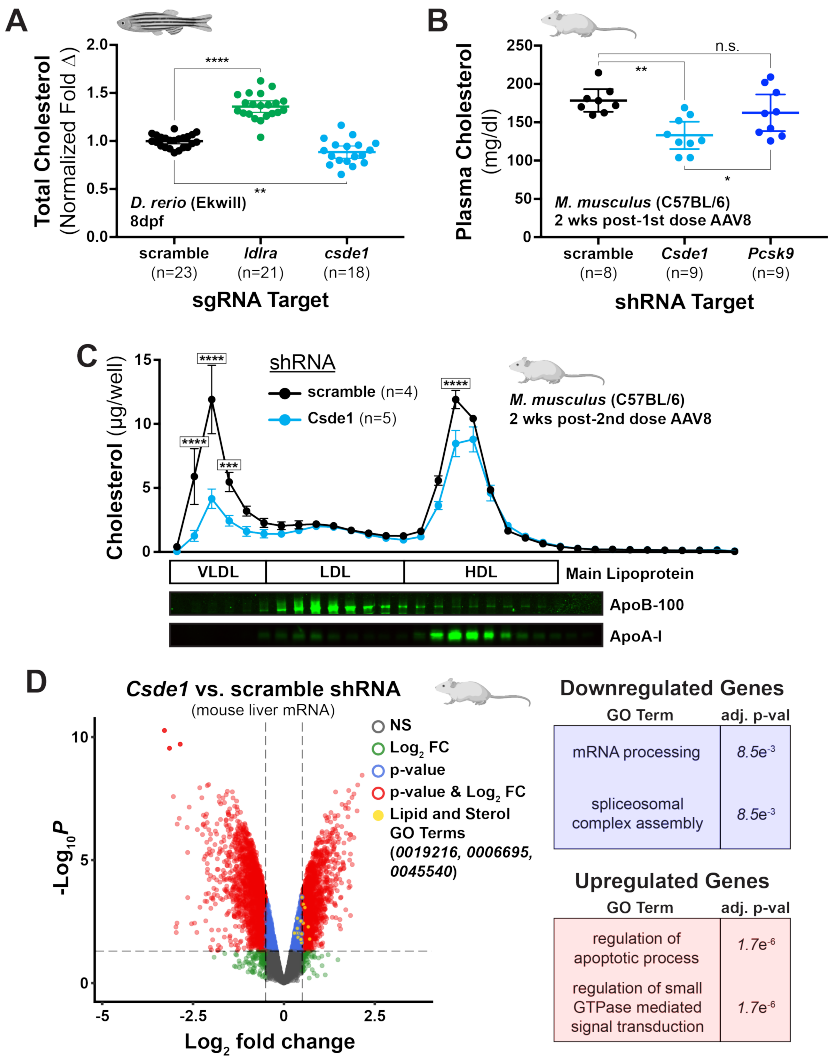

Figure 5: CSDE1 Disruption Upregulates the LDLR *in vivo*. *A)* Total cholesterol, in µg cholesterol per mg of total protein, of homogenates of 8 days post fertilization (dpf) zebrafish larvae fed a high-cholesterol diet and subjected to Cas9 mediated gene disruption of indicated target. Data are normalized to the scramble control of a particular experiment. Each point represents a homogenate consisting of 10 larvae. Data represent summary information from 4 independent experiments. One-way ANOVA with Holm-Sidak's multiple comparisons test shown. *B)* Total fasting plasma cholesterol of C57BL/6 mice on an atherogenic diet, 2 weeks after transduction with AAV8-packaged shRNA against indicated target. Each point represents an individual mouse. One-way ANOVA with Tukey's multiple comparisons test shown. Error bars = 95% confidence intervals. *C)* Cholesterol levels of fractions collected from gel filtration of plasma from individual mice, harvested 2 weeks after transduction with second dose of AAV8-packaged shRNA. Note that fractions shown begin with the elution front from the size-exclusion column. Each dot represents the mean cholesterol level from mice in the same intervention arm. Immunoblots from representative fractions against mouse ApoB-100 and ApoA-I shown below. Two-way ANOVA with Sidak's multiple comparisons test shown to illustrate comparison between treatment arm within a given fraction. Error bars = standard error of the mean. *D)* Volcano plot showing differentially expressed genes between *Csde1* and scramble shRNA treatment arms, filtered for effects of viral transduction. Statistical significance is shown on the y

axis and strength of effect is shown on the x axis. Comparison made among the 3 mice in each arm with the highest *eGFP* transcript expression, as a proxy for transduction efficiency. Genes reaching threshold significance for p-value (blue), $\log_2$ fold change (green), both (red), or neither (grey) annotated accordingly. Genes associated with lipid and sterol metabolic GO terms highlighted in yellow (0019216 = lipid metabolic process, 000695 = cholesterol biosynthetic process, and 0045540 = regulation of cholesterol biosynthetic process). Leading upregulated and downregulated GO terms of all statistically significant differentially expressed genes noted in the boxes at right. *All panels)* n.s. = non-significant, * = $p < 0.05$, ** = $p < 0.01$, *** = $p < 0.001$, and **** = $p < 0.0001$.

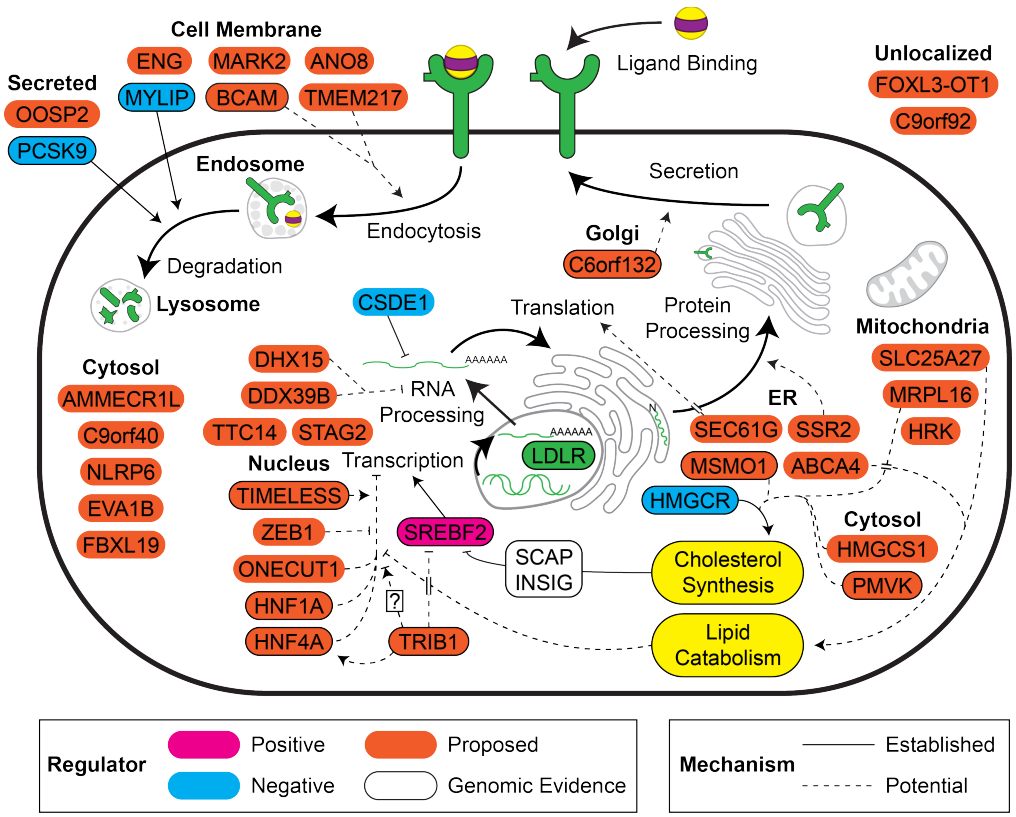

Figure 6: An Exploratory Map of Potential LDLR Regulatory Targets. Genes identified and validated in the screen are mapped by cellular localization and possible mechanisms of effect. Known downregulators are shown in cyan (including CSDE1 given the results presented in the current study) and known upregulators shown in magenta. Validated hits with observed effects on cell proliferation or viability are excluded.

1493 **Tables and Table Legends**
1494

Hit	Hit (NCBI Name)
ABCA1	ABCA1
ABCA4	ABCA4
ACAN	ACAN
ALKBH5	ALKBH5
AMMECR1L	AMMECR1L
ANO8	ANO8
BCAR1	BCAR1
C12orf45	C12orf45
C14orf79	CLBA1
C1orf210	C1orf210
C5orf34	C5orf34
C6orf132	C6orf132
C9orf40	C9orf40
C9orf92	C9orf92
CD164L2	CD164L2
CD276	CD276
CD96	CD96
CIT	CIT
CSDE1	CSDE1
CXCR2	CXCR2
CXXC11	FBXL19
CYB5R3	CYB5R3
DDX39B	DDX39B
DESI1	DESI1
DHX15	DHX15
DUOX1	DUOX1
EIF3D	EIF3D
ENG	ENG
ENTPD1	ENTPD1
ESRRG	ESRRG
EVA1B	EVA1B
FAM126A	FAM126A
FAM178B	FAM178B
FAM57A	TLCD3A
FBXW11	FBXW11
FDPS	FDPS

GXYLT1	GXYLT1
HMGCR	HMGCR
HMGCS1	HMGCS1
HNF1A	HNF1A
HNF4A	HNF4A
HPGDS	HPGDS
HRK	HRK
ICAM4	ICAM4
INTS8	INTS8
ITGA11	ITGA11
ITGA7	ITGA7
ITGAV	ITGAV
LDLR	LDLR
LGALS14	LGALS14
LOC100288524	FOXL3-OT1
LOC729159	NPAP1L
LYZ	LYZ
MARK2	MARK2
MATN1	MATN1
MFHAS1	MFHAS1
MRAP2	MRAP2
MRPL16	MRPL16
MRPL22	MRPL22
MSMO1	MSMO1
MYLIP	MYLIP
NCR2	NCR2
NDUFB5	NDUFB5
NDUFS8	NDUFS8
NINJ1	NINJ1
NLRP6	NLRP6
ONECUT1	ONECUT1
OR52A1	OR52A1
PCDH7	PCDH7
PCDHB4	PCDHB4
PCSK9	PCSK9
PHGR1	PHGR1
PIANP	PIANP
PID1	PID1
PLAC1L	OOSP2

PMVK	PMVK
POLD2	POLD2
POLD3	POLD3
PRIM1	PRIM1
PROL1	OPRPN
PTGDR2	PTGDR2
RARRES3	PLAAT4
REPS1	REPS1
RNF151	RNF151
RSG1	CPLANE2
SCUBE1	SCUBE1
SEC61G	SEC61G
SERPINA9	SERPINA9
SF3A2	SF3A2
SLC25A27	SLC25A27
SLC2A7	SLC2A7
SLC6A19	SLC6A19
SLURP1	SLURP1
SMURF1	SMURF1
SON	SON
SREBF2	SREBF2
SSR2	SSR2
SSUH2	SSUH2
ST6GALNAC4	ST6GALNAC4
STAC	STAC
STAG2	STAG2
TIMELESS	TIMELESS
TMEM217	TMEM217
TMEM86A	TMEM86A
TPRG1	TPRG1
TRMT10C	TRMT10C
TRPM1	TRPM1
TRPM7	TRPM7
TTC14	TTC14
TXNDC8	TXNDC8
WDR5	WDR5
WDR75	WDR75
ZBED6CL	ZBED6CL
ZBTB42	ZBTB42

ZC3H12A	ZC3H12A
ZEB1	ZEB1
ZNF595	ZNF595

Table 1: LDLR Specific CRISPRi Screen Hits. Hits are listed both by gene name in the genome-wide library*(14)* as well as NCBI name.

GENE	Variant rsID	BETA	P_BOLT_LMM	Consequence	IMPACT
HNF4A	rs1800961	0.0564144	0	missense_variant	MODERATE
BCAM	rs28399659	-0.0174111	7.70E-29	missense_variant	MODERATE
BCAM	rs200398713	-0.0803165	1.80E-28	splice_region_variant,intron_variant	LOW
BCAM	rs199922856	-0.342179	6.20E-28	missense_variant	MODERATE
BCAM	rs28399654	0.220592	6.10E-10	missense_variant	MODERATE
BCAM	rs3810141	0.020077	5.50E-07	stop_gained	HIGH
TIMELESS	rs2291738	0.00388393	0.00014	splice_region_variant,intron_variant	LOW
BCAM	rs149302547	-0.147327	0.005	missense_variant	MODERATE
BCAM	rs1135062	-0.0213642	0.0074	missense_variant	MODERATE
C6orf132	rs55772414	0.0116856	0.013	missense_variant	MODERATE
MSMO1	rs142496142	0.0432195	0.015	missense_variant	MODERATE

Table 2: Association of Nonsynonymous Variants in CRISPRi Screen Hits with Serum LDL-C in the UK Biobank. BETA indicates the linear regression standardized effect size, and P_BOLT_LMM indicates the linear mixed model p value using BOLT-LMM*(97)*.

Supplementary Figures and Figure Legends

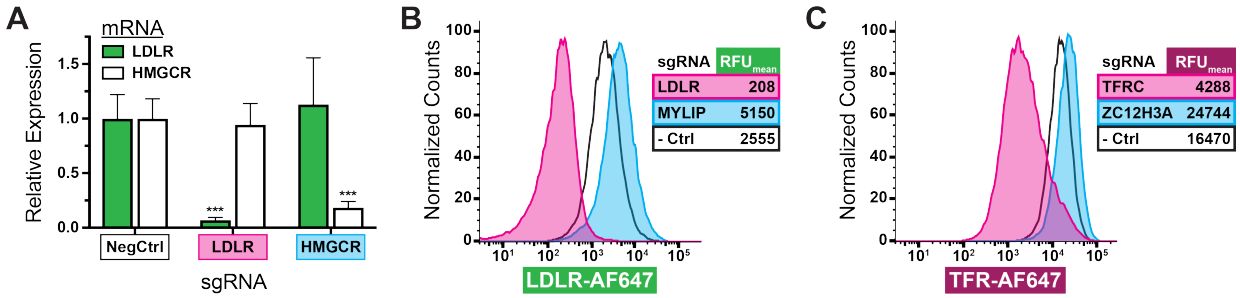

Supplementary Figure 1: Validation of dCas9-KRAB-HepG2 Cells. *A)* Relative expression, by qPCR, of *LDLR* and *HMGCR* in engineered dCas9-KRAB HepG2 cells transduced with sgRNAs targeting the indicated genes. *B2M* used as qPCR control. Error bars indicate 95% confidence intervals. *** = $p < 0.001$ by Holm-Sidak corrected T-test, comparing to negative control sgRNA of the same target. *B)* Flow cytometry analysis, by surface labelling with anti-LDLR-AF647, of dCas9-KRAB HepG2 cells transduced with sgRNAs targeting the indicated genes. Mean fluorescence shown in inset. *MYLIP* (IDOL) is an E3 ligase which ubiquitinates the LDLR, leading to lysosomal degradation*(26)*. *C)* Flow cytometry analysis as in *B* but transduced with indicated sgRNAs and labelled with anti-TFR-AF647. *ZC3H12A* (REG1) is an endoribonuclease that accelerates the degradation of TFR mRNA*(27)*.

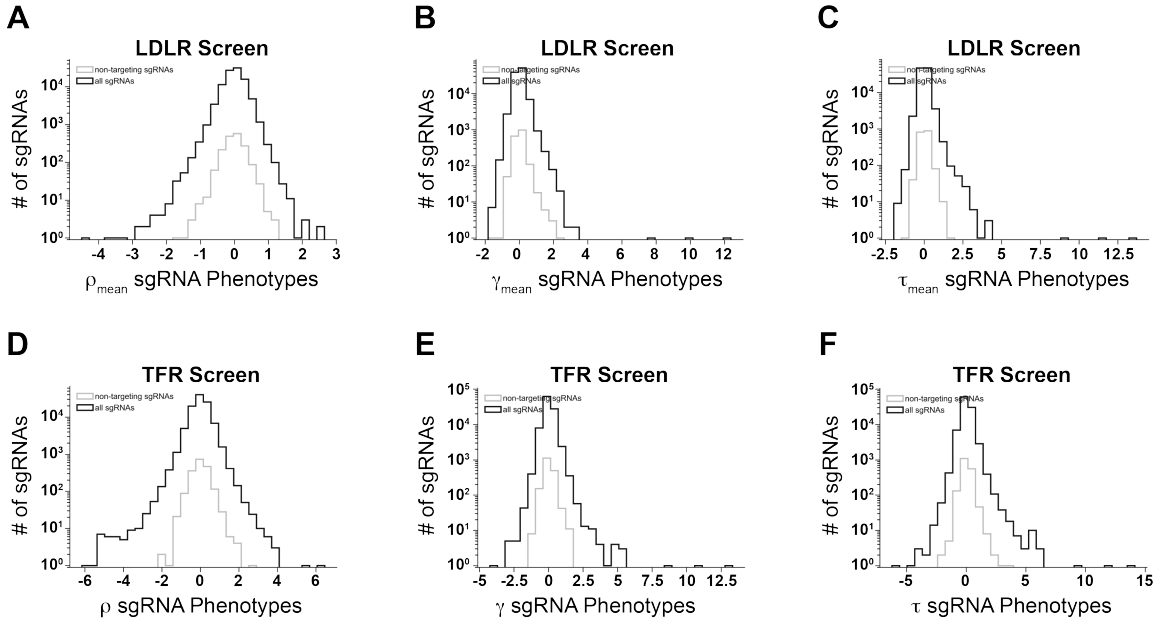

Supplementary Figure 2: Recovered sgRNAs from Screening Phenotypes. Distribution of number of guide RNAs recovered by phenotype in both LDLR (*A-C*) and TFR (*D-F*) screens. ρ (*A,D*) indicates $\log_2$ fold enrichment for sgRNA in high receptor abundance cells compared to low receptor abundance cells. γ (*B,E*) indicates $\log_2$ enrichment for sgRNA in low receptor abundance cells compared to unsorted population. τ (*C,F*) indicates $\log_2$ enrichment for sgRNA in high receptor abundance cells compared to unsorted population. Mean results are reported for the 3 replicates of the LDLR screen (*A-C*).

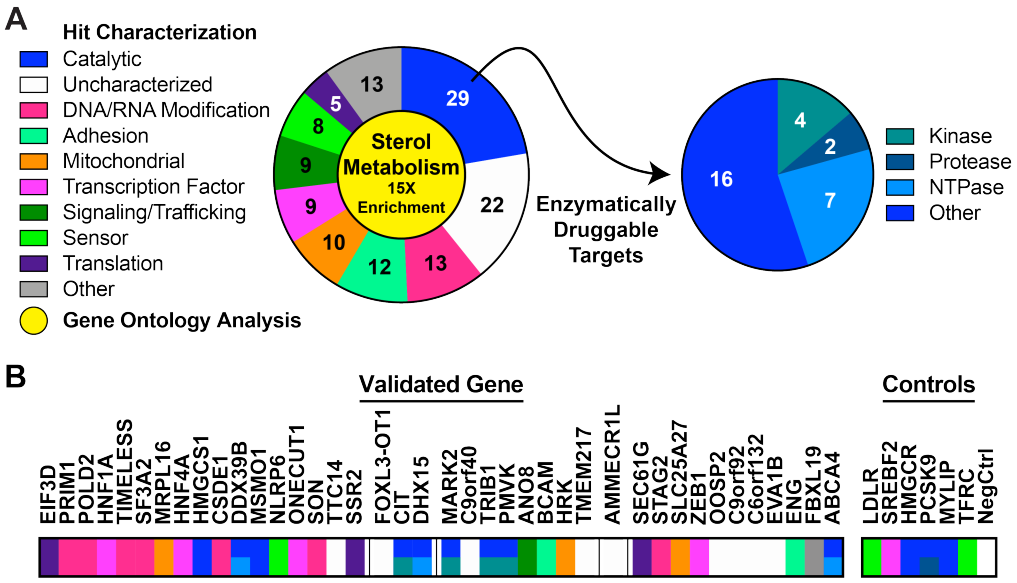

Supplementary Figure 3: Gene Ontology and Localization Analysis. *A)* Characterization of hits from the LDLR screen based on gene ontology (GO) and localization, along with results from GO enrichment analysis (yellow center). Note that multiple genes fall into more than one category. *B)* Primary classification of the 40 LDLR hits independently validated outside of the pooled screen and displayed, as in Fig. 2, according to the color codes in *A*.

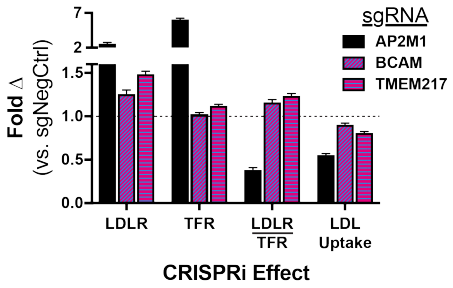

Supplementary Figure 4: Selective LDLR Effect of Transmembrane Proteins. Flow cytometric readout of receptor abundance and LDLR function assays, using CRISPRi knockdowns against genes thought to be involved in endocytosis. Data, which represents 3 to 4 independent experiments, are normalized to readout of negative control sgRNA within each experiment. Error bars represent 95% confidence intervals. Note the discontinuous Y axis.

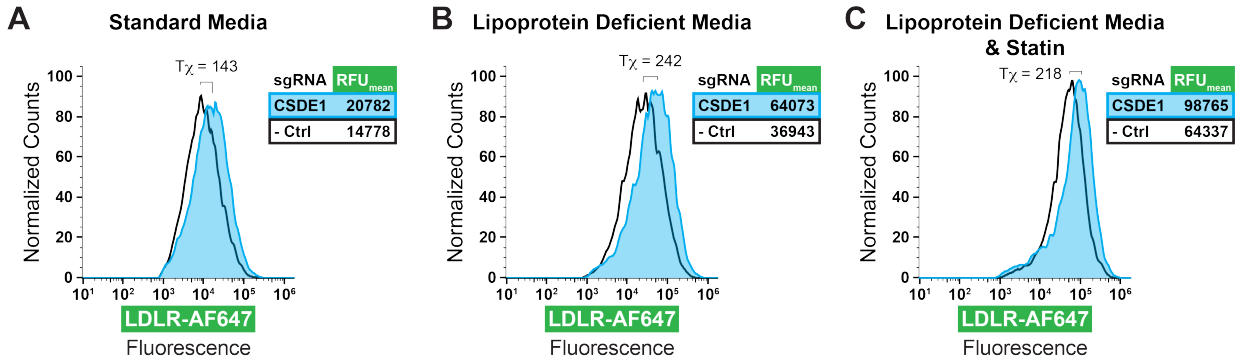

Supplementary Figure 5: Effect of Sterol Conditions on CSDE1 Knockdown. Flow cytometry histograms showing AF647 conjugated anti-LDLR antibody labelling (as proxy for LDLR abundance) of engineered dCas9-KRAB HepG2 cells transduced with indicated sgRNAs and grown in standard growth media (*A*), lipoprotein-deficient media (*B*), or lipoprotein deficient media with a concomitant statin (*C*). Tχ metric (FlowJo v10)*(105–107)* shown on graph, and mean fluorescence shown in insets.

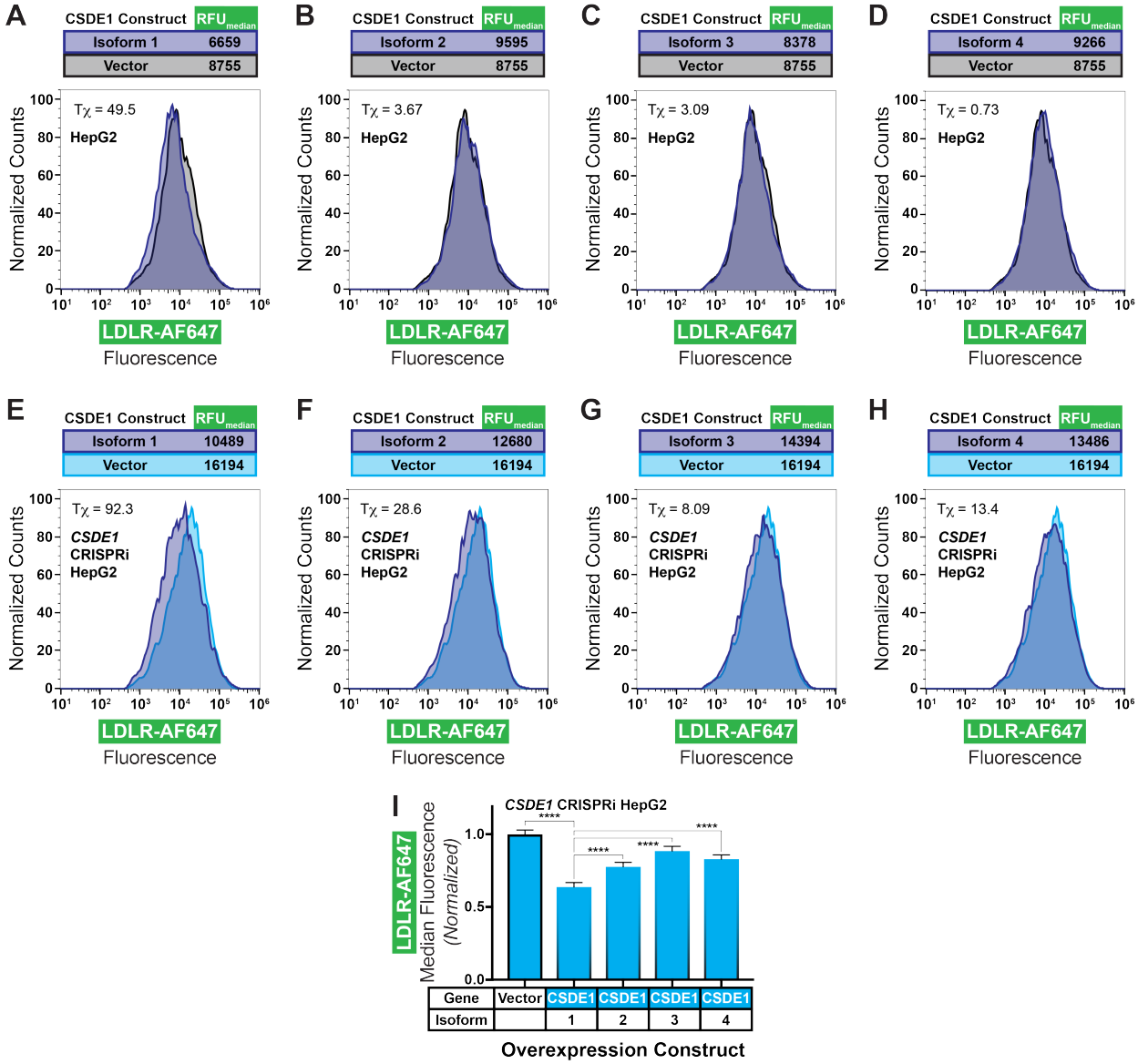

Supplementary Figure 6: Effect of CSDE1 Overexpression. Flow cytometry histograms showing AF647 conjugated anti-LDLR antibody labelling (as proxy for LDLR abundance) of HepG2 cells (*A-D*) or engineered dCas9-KRAB HepG2 cells transduced with *CSDE1* targeting sgRNA (*E-H*) and transfected with an overexpression construct encoding the indicated CSDE1 isoform or vector alone. Tχ metric (FlowJo v10)*(105–107)* shown on graphs, and median fluorescence shown above. Quantified relative LDLR abundance of normalized median fluorescence of the data from *e-h* shown in *i*, with one-way ANOVA with Tukey's multiple comparisons test. Error bars indicate 95% confidence intervals. **** = $p < 0.0001$.

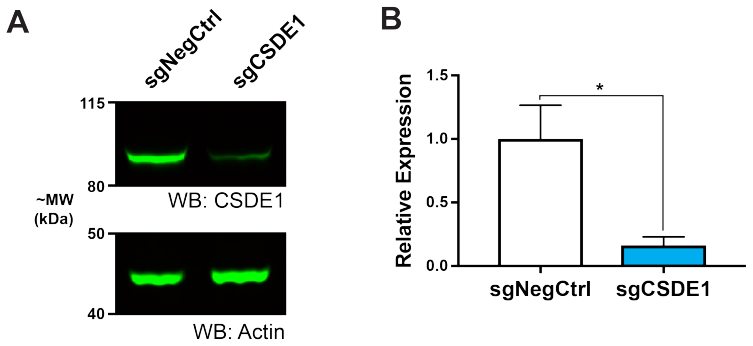

Supplementary Figure 7: CSDE1 Knockdown at Protein Level. *A*) Representative immunoblots of lysates of dCas9-KRAB HepG2 cells harboring indicated guide RNA. CSDE1 shown above, and β-actin (loading control) shown below. *B*) Quantification of relative abundance of CSDE1 (normalized to loading control) shown in immunoblot in *A*. Data includes 3 independent experiments. * indicates $p < 0.05$ by Welch's T-test.

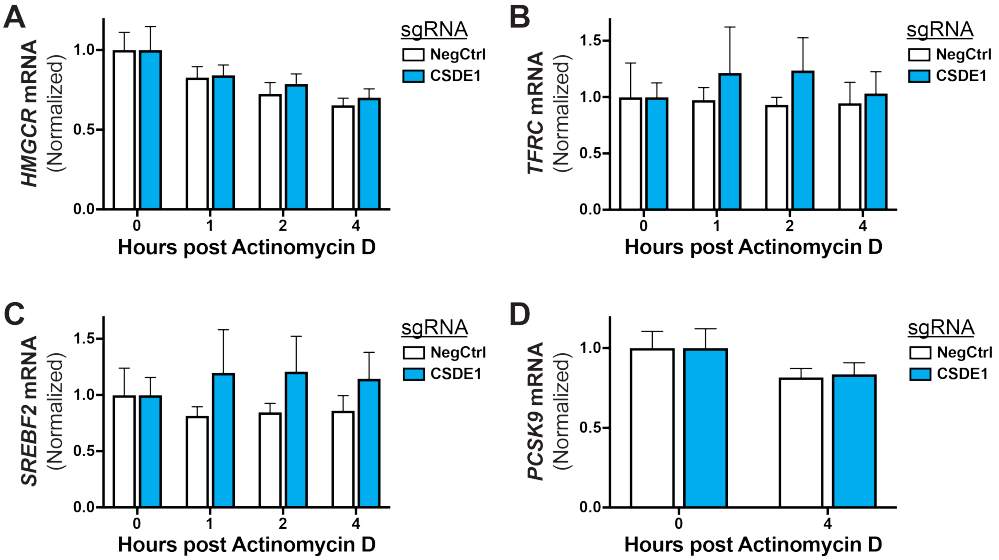

Supplementary Figure 8: Effect of *CSDE1* Knockdown on Decay of Non-*LDLR* Transcripts. Relative expression, by qPCR, of *HMGCR (A), TFRC (B), SREBF2 (C), or PCSK9 (D)* mRNA in dCas9-KRAB HepG2 cells transduced with indicated sgRNAs and subjected to arrest of transcription with actinomycin D. Data are normalized to results at T=0 within the sgRNA evaluated to illustrate the change in time. Data represent summary results from 3 independent experiments. Error bars = 95% confidence intervals. All pairwise comparisons (unpaired t-tests with Holm-Sidak correction) are nonsignificant.

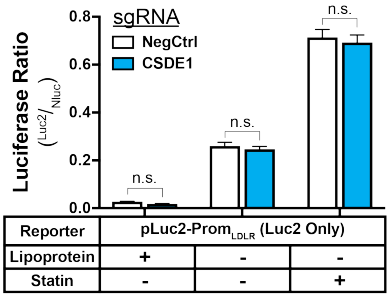

1583
1584
1585 **Supplementary Figure 9: Physiologic Response of Luciferase Reporter System.** Relative
1586 ratiometric luciferase activity of dCas9-KRAB HepG2 (CRISPRi) cells transiently transfected
1587 with unmodified Luc2 construct under the *LDLR* promoter (pLuc2-Prom$_{LDLR}$, Fig. 4E) and
1588 secreted Nluc reporter under the CMV promoter and subjected to indicated media conditions.
1589 Data represent summary results from 3 independent experiments. n.s. = non-significant. Two-
1590 way ANOVA with Sidak's multiple comparisons test was used.
1591

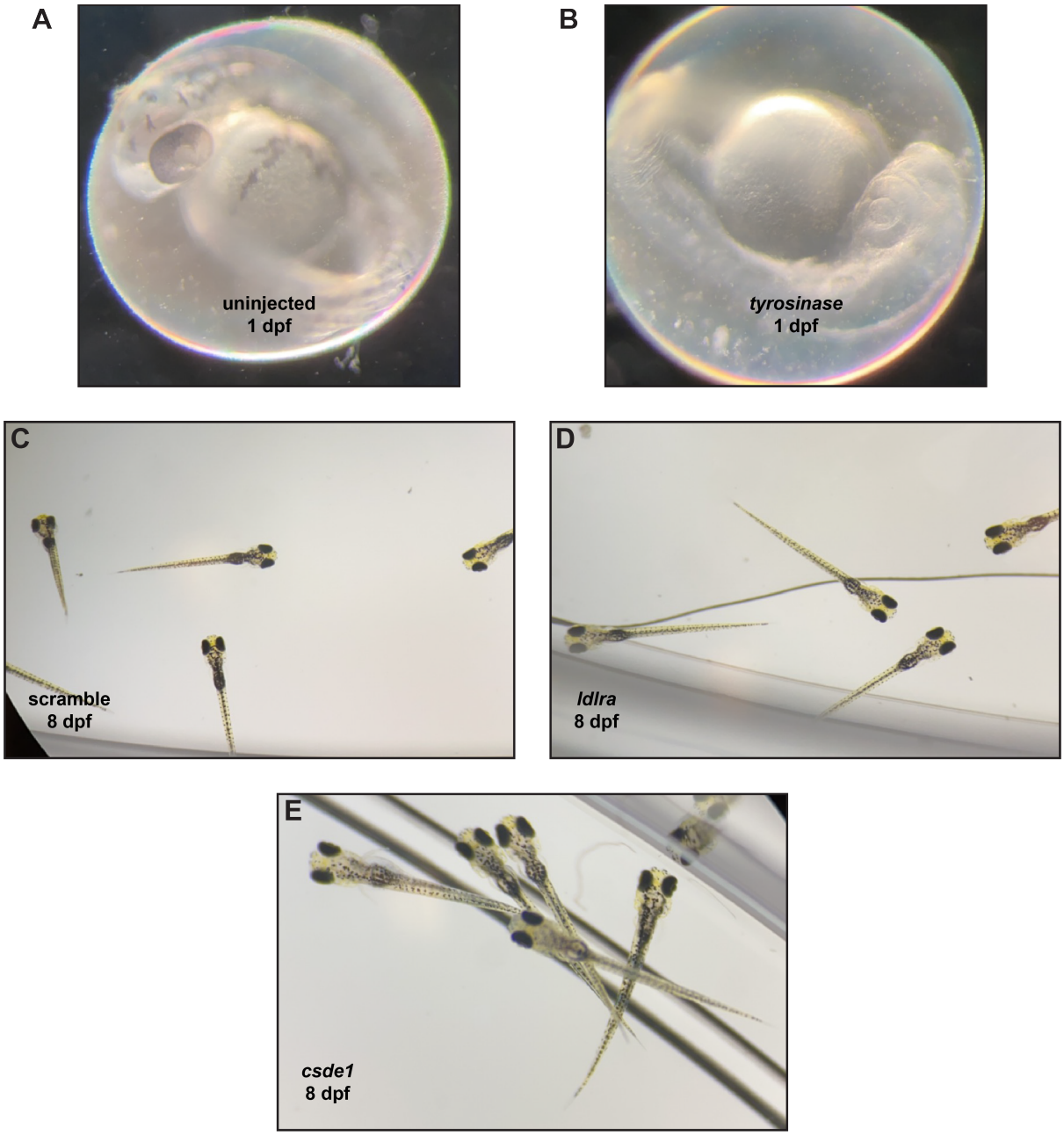

Supplementary Figure 10: Visual Phenotypes of Zebrafish Cas9-sgRNA Saturation Gene Disruption. *A,B*) Representative microscopic images of zebrafish larvae at 1 day post fertilization without (*A*) or with (*B*) injected Cas9 and redundant guides against tyrosinase control performed concomitantly with each zebrafish experiment. Albinism is the readout for successful injections. *C-E)* Representative microscopic images of zebrafish larvae at 8 dpf and with injected Cas9 and guides against scramble controls (*C*), *ldlra* (*D*), and *csde1* (*E*).

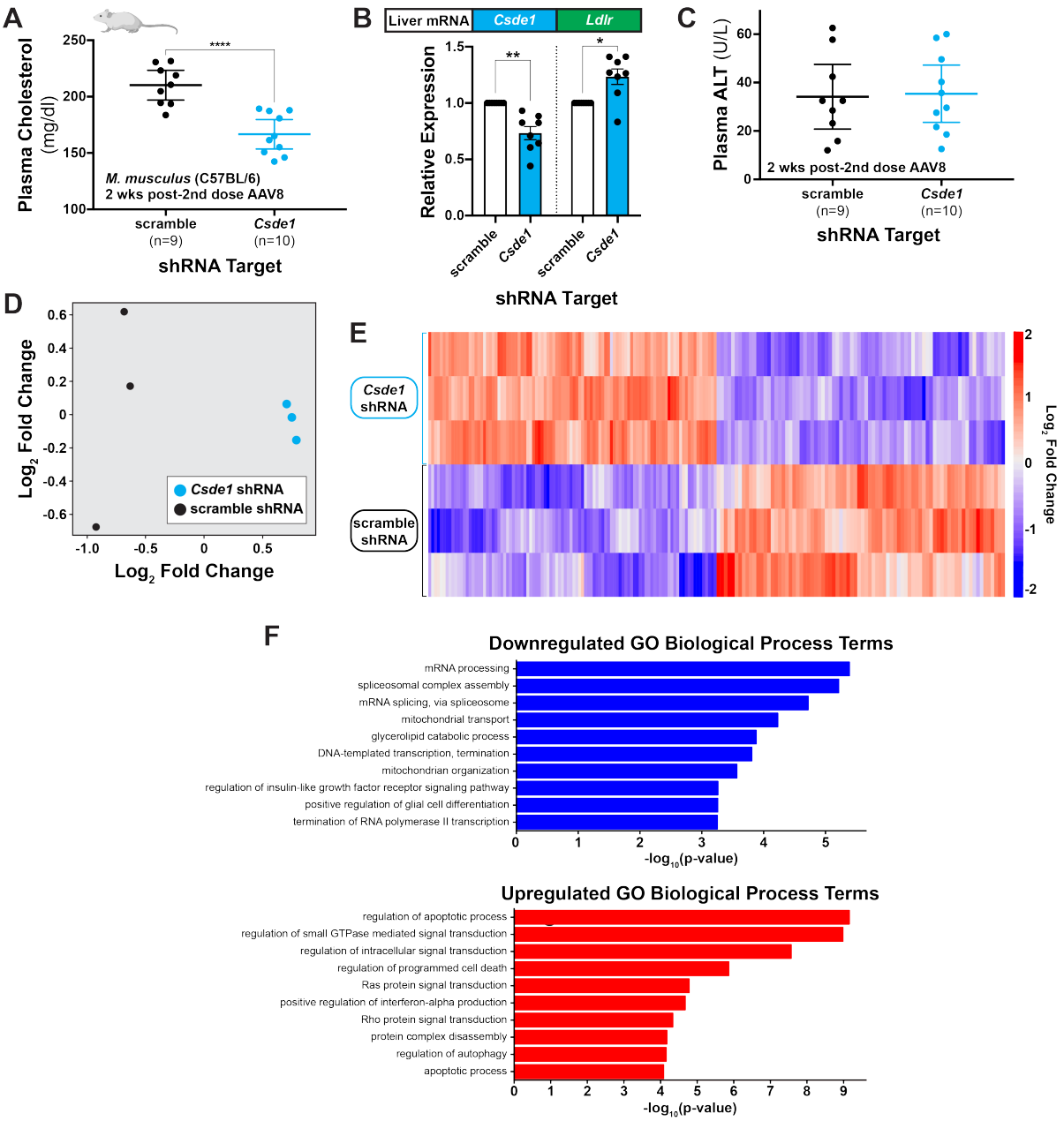

Supplementary Figure 11: Effects of *in vivo Csde1* Disruption in Mice. *A)* Total fasting plasma cholesterol of C57BL/6 mice on an atherogenic diet, 2 weeks after transduction with second dose of AAV8-packaged shRNA against indicated target (8 weeks after first dose). Welch's t-test shown. *B)* Relative expression, by qPCR, of indicated mRNA targets from mouse liver tissue from the indicated treatment arms. Expression normalized to *B2m* as the housekeeping control. Welch's T-test shown. Error bars = standard error of the mean. *C)* Plasma alanine aminotransferase activity (ALT) of mice from *A*. Welch's T-test revealed no significant difference between intervention arms. *D)* Unsupervised cluster analysis of individual mice analyzed for differential gene analysis. *E)* Heatmap of top 100 differentially expressed genes (by p value) of the individual mice analyzed by RNA-seq. Mice transduced with AAV8-scramble-shRNA at the bottom and those transduced with AAV8-*Csde1*-shRNA at the top. *F)* Top 10 biological process GO terms (by uncorrected p value) identified from all statistically

1615 significant differentially expressed genes downregulated (blue) or upregulated (red) by *Csde1*
1616 shRNA treatment. *All)* Each data point represents an individual mouse. * = $p < 0.05$, ** = $p <$
1617 0.01, and **** = $p < 0.001$. Error bars = 95% confidence intervals unless noted otherwise.
1618

Metric	Value
Age (y)	56.9 (7.9)
Sex	179,963 (46.1%)
European ancestry	376,358 (96.4%)
Cholesterol (mg/dl)	
Total	221.1 (44.3)
HDL	56.1 (14.8)
LDL	138.1 (33.7)
Triglycerides (mg/dl)	132.6 [93.6-191.5]
Statin Rx	64,004 (16.4%)
BMI (kg/m^2)	27.4 (4.8)
Systolic blood pressure (mmHg)	140.2 (19.7)
Diastolic blood pressure (mmHg)	82.3 (10.7)
Current smoker	39,736 (10.2%)
Diabetes mellitus type 2	25,349 (6.5%)
Coronary artery disease	18,204 (4.8%)

Supplementary Table 7: Baseline Characteristics of UK Biobank Participants in Genomic Association Analyses. Continuous values are presented as mean (standard deviation) except for triglycerides which is given as median (Q1-Q3) due to the skewness of the triglyceride distribution. Categorical data are presented as count (percentage). BMI = body-mass index; HDL = high-density lipoprotein; LDL = low-density lipoprotein.